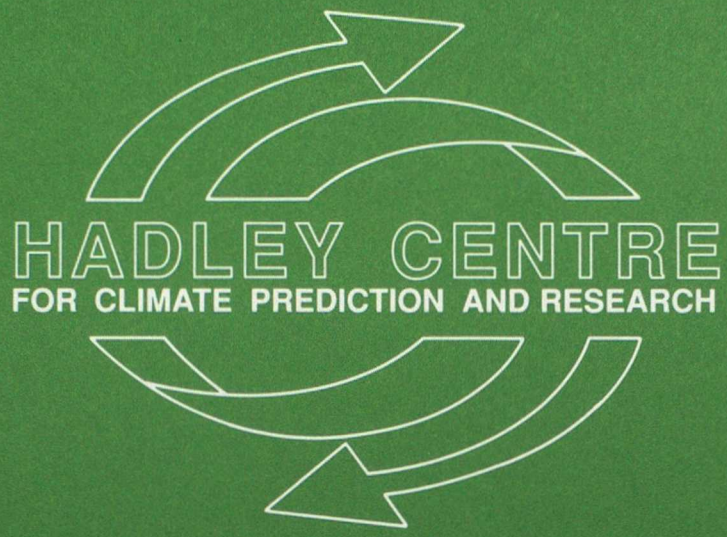

Sea-level changes under increasing atmospheric CO_2 in a transient coupled ocean-atmosphere GCM experiment

by

J.M.Gregory

CRTN 42

November 1993

CLIMATE
RESEARCH
TECHNICAL
NOTE

Hadley Centre
Meteorological Office
London Road
Bracknell
Berkshire RG12 2SY

CLIMATE RESEARCH TECHNICAL NOTE NO. 42

SEA-LEVEL CHANGES UNDER INCREASING ATMOSPHERIC CO_2 IN A TRANSIENT COUPLED OCEAN-ATMOSPHERE GCM EXPERIMENT

by

J M Gregory

November 1993

Hadley Centre for Climate Prediction and Research
Meteorological Office
London Road
Bracknell
Berkshire RG12 2SY

NOTE: This paper has not been published. Permission to quote from it should be obtained from the Director of the Hadley Centre.

Abstract

Climate change resulting from the enhanced greenhouse effect of increasing atmospheric CO_2 concentrations is expected to bring about global and local changes in sea-level. A global rise in sea-level would result from thermal expansion of sea-water and from melting of land ice, while changes in ocean dynamics and atmospheric pressure patterns could alter relative sea-surface topography. Global and local sea-level changes have been diagnosed from a 75-year experiment with a version of the UK Meterological Office coupled ocean–atmosphere general circulation model in which the CO_2 concentration increases at 1% per year. Over the final decade, the component of mean global-average sea-level rise caused by thermal expansion is 90 mm; on this timescale, a significant contribution is expected from melting of mountain glaciers, but the model does not represent these. Sea-level rises over practically the entire ocean area, but there is considerable variation in the magnitude, showing that the global figure by itself gives only a rough idea of the local effect; the largest rises are found in the north-west Atlantic. We illustrate how this local variation makes it difficult to estimate global sea-level rise from a limited number of coastal stations, as usually has to be done in practice.

1 Introduction

It is generally expected that increasing atmospheric concentrations of greenhouse gases, especially CO_2, will lead in the next few decades to significant change to the climates of the world (IPCC, 1990). A probable consequence of this would be alterations in local and global sea-level. Predictions of sea-level change, especially sea-level rise, are of considerable importance because of the social and economic impacts of such changes, in particular on populations which inhabit low-lying areas.

Contributions to sea-level changes can arise from changes in any of the components of the climate system, namely through

- Expansion or contraction of sea-water, as a response to changes in temperature and salinity, *i.e.* alterations to the density of water in the oceans;
- Modification to the water balance (atmosphere, ocean, land, ice), *i.e.* alterations to the mass of water in the oceans, the most important effect on the timescale of decades being retreat or advance of mountain glaciers;
- Changes in ocean circulation.
- Changes in sea-level atmospheric pressure.

The first two of these determine the global mean sea-level (through the total volume of water in the oceans). The last two have to be considered to deduce local sea-level (the way this volume is spread over the ocean area).

Thus, in order to model sea-level changes, the complete climate system must be considered. Much of the work that has been done hitherto on this subject employs a one-dimensional box upwelling–diffusion climate model (IPCC, 1990; Wigley and Raper, 1987). This model represents the vertical profile of area-averaged ocean temperature, which changes in response to changes in radiative flux at the surface computed from greenhouse-gas scenarios. Thermal expansion of sea-water is diagnosed from the temperature profile, and a parameterisation of glacier melt is included which depends on the ocean surface temperature, taken to be representative of average surface air temperature. One advantage of such a model is that it is very cheap in computer time, and estimates have been produced of global-average sea-level rise for a variety of scenarios. The scenarios and the results take the form of time-series starting from a notional "present day" or some defined time in the past.

However, information about local sea-level changes cannot be obtained by this means. For this purpose a three-dimensional ocean model is needed, and some such results have been published. Mikolajewicz *et al.* (1990) have used an ocean general circulation model (OGCM) to

compute changes in local sea-surface topography (only the thermal-expansion component) which would be consequent on imposed time-dependent surface air temperature changes caused by progressively increasing atmospheric CO_2. The surface temperature forcing is estimated from an average of the results of a number of equilibrium double-CO_2 atmospheric general circulation model (AGCM) experiments. Church *et al.* (1990) made a calculation of the effects of surface temperature changes using a method in which heat is introduced into the ocean by advection along isopycnal surfaces, and there is a subsequent adjustment to the new temperature structure through the mechanism of internal waves, which redistributes the extra volume resulting from thermal expansion. They used spatial distributions of temperature changes expected by 2050, again from AGCM results. Thus, both of these pieces of work present the ocean response to prescribed atmospheric temperature changes.

A more satisfactory way to obtain the time-dependent local sea-level response of the ocean to a changing climate is to use a coupled ocean–atmosphere climate model. In such a model, changes in the ocean and atmosphere feed back on each other as the climate evolves. Owing to limitations on computing resources, not many experiments have been run with coupled models: some results for sea-level changes are available (and mentioned in Sections 3.1 and 4.2) from experiments conducted at the Geophysical Fluid Dynamics Laboratory, Princeton (IPCC, 1992), the Max-Planck-Institut für Meteorologie, Hamburg (Cubasch *et al.*, 1992a, 1992b), and the UK Meteorological Office, as described in this paper.

2 The model and the experiment

A version of the Meteorological Office climate model has recently been used to undertake a transient climate-change experiment (Murphy, 1992), *i.e.* one in which atmospheric CO_2 levels are gradually increased. The climate model comprises coupled ocean and atmosphere general circulation models. The atmosphere GCM is a finite-difference grid-point model based on the primitive equations, incorporating parameterisations of penetrative convection (Gregory and Rowntree, 1990), land surface (Warrilow and Buckley, 1989) and gravity-wave drag (Palmer *et al.*, 1986) and using a prognostic cloud scheme with a cloud liquid-water variable (Smith, 1990). The ocean GCM is also a finite-difference grid-point model, a version of the Cox GFDL ocean code (Cox, 1984), including stability-dependent vertical mixing (Pacanowski and Philander, 1981), isopycnal diffusion (Redi, 1982), a representation of the mixed layer (Kraus and Turner, 1967) and a thermodynamic sea-ice model (Semtner, 1976). The spatial resolution used for both atmosphere and ocean was $2\frac{1}{2}^\circ$ of latitude by $3\frac{3}{4}^\circ$ of longitude; the atmosphere model had 11 irregularly spaced levels in the vertical, and the ocean 17. The two were run asynchronously, with coupling fields being exchanged at five-day intervals. Both components are more fully described by Murphy (1992).

The transient climate-change experiment consisted of two 75-year integrations, serving as control and anomaly, from the same initial state. The atmospheric CO_2 concentration remained constant throughout the control, and increased at 1% a^{-1} compounded in the anomaly. This scenario gives a doubling of CO_2 by year 70. In order to prevent the climate of the control run from drifting far from climatology, corrective fluxes of heat and water had to be applied at the ocean–atmosphere interface. The same fluxes were applied in the anomaly integration. For details of this procedure, see Murphy (1992). By year 75, the global-average temperature rise (anomaly – control) was $\sim 1{\cdot}7\,^\circ$C. From previous equilibrium climate-change experiments with a similar atmospheric model coupled to a slab ocean, and from a simple energy-balance model, the climate sensitivity of the coupled model (equilibrium temperature change for a doubling of atmospheric CO_2) is estimated to be $+2{\cdot}7\,^\circ$C. The observed warming is less than this because the climate system is not in equilibrium at the end of the transient experiment.

From the output of this experiment, global and local sea-level changes have been diagnosed. However, it should be noted that the climate model was not specifically designed with the intention of calculating sea-level changes. We will discuss several deficiencies it has in regard to this particular purpose which are tolerable in general because they are of little importance

for climate modelling. Though some of these deficiencies of our model are important, it should be stressed that the same shortcomings are present in some or all of the other coupled ocean–atmosphere models currently in use.

In the following sections, we consider each of the influences on sea-level listed above. We make clear what the model can and cannot do adequately. With regard to the latter, this work does at least point out what is required, and it indicates a methodology for a more complete calculation.

3 Global sea-level rise

3.1 Thermal expansion

The most obvious difficulty in diagnosing sea-level changes from the Cox ocean model is that it does not directly give any information at all about sea-surface because it uses the rigid-lid approximation, in order to suppress surface waves. That is, the sea has a fixed surface $z = 0$, coinciding with the mean sea-surface of the real ocean. (The dynamical effect of this arrangement will be discussed in Section 4.1 and the Appendix.) Despite this, it is possible to extract information from the model about the implied sea-level, as will be shown.

The fields of temperature $T(x, y, z)$ and salinity $S(x, y, z)$ are prognostic variables of the model. From them, the field of density ρ can be calculated using the equation of state, which is represented by a parameterisation based on that of Fofonoff. The effect of pressure is included approximately by using different sets of coefficients dependent on model level, *i.e.* depth, but not on location. We can calculate the total mass of the model ocean,

$$M = \oint_A \int_{-H}^{0} \rho \, \mathrm{d}z \, \mathrm{d}A, \tag{1}$$

where $H(x, y)$ is the depth of the ocean, z being positive upwards, A is the horizontal sea-surface and $\rho = \rho(T(x, y, z), S(x, y, z), p(z)) = \rho(x, y, z)$. It is clear that, since H is constant, M is not; *i.e.* the ocean model does not conserve water. It is possible for this to happen because of the form in which the continuity equation is used. Conservation of mass would require $\nabla \cdot (\rho \mathbf{u}) = 0$, but in the Boussinesq approximation the density is taken to be constant except in terms involving buoyancy forces. Hence continuity assumes the form $\nabla \cdot \mathbf{u} = 0$, which neglects the advection of density.

Since equation (1) is linear, the change in mass of the ocean between one state and another is

$$\Delta M = \oint_A \int_{-H}^{0} \Delta\rho \, \mathrm{d}z \, \mathrm{d}A.$$

In this way we can find the difference in M between year 1 and year y of the transient integration, for instance. However, we do not suppose that the mass of the real ocean will actually change greatly over time. (This is confirmed in the next section, where we investigate the possible changes in mass.) What actually happens when the density structure of the ocean changes is that its volume V will alter. If ΔM is relatively small, we can use the result of the fixed-volume rigid-lid ocean model to estimate the corresponding volume change of the real ocean as $\Delta V = -\Delta M / \rho$.

Since the extra volume ΔV is not represented in the model, in principle we have no information about how it is distributed. However, it seems sensible to assume that changes in local T and S lead to expansion and contraction more or less *in situ*. (In the Appendix we will examine how accurate this is.) In that case, the appropriate density to use in computing ΔV is the local density, and

$$\Delta V = -\oint_A \int_{-H}^{0} \frac{\Delta\rho}{\rho} \, \mathrm{d}z \, \mathrm{d}A. \tag{2}$$

This suggests another way to state the requirement for the rigid-lid approximation to be valid, namely that the expansion of a given layer must be small compared with its thickness, so that the same vertical coordinate z is applicable to the layer in both states.

Since the equation of state for sea-water is non-linear in salinity (and temperature), changing the distribution in the ocean of a fixed mass of salt could alter the total volume and the average sea-level. This effect, however, is very small. What does have to be taken into account is that the model does not exactly conserve salt, because this could lead to significant alterations to sea-level (about 5% of the effect of thermal expansion in practice). The simplest way to compensate for it is to exclude changes in salinity from the calculation of density.

Using annual-mean fields of T and S, annual values for ΔV compared with the initial volume were computed for years 2–75 in both control and anomaly integrations, and divided by the total ocean surface area A in order to convert them to sea-level rise $d = \Delta V/A$. Since the temperature changes involved are O(K) and the cubic expansivity of water is O(10^{-4}) K^{-1}, the fractional volumetric expansion will be O(10^{-4}). The warming, as will be shown, is generally confined to the top few 100 m of the ocean. We therefore expect a sea-level rise of a few cm, which is indeed what is calculated.

The control run exhibits a sea-level rise of 111 mm by year 75. This happens partly because there is a climate drift in the control run, mostly in the southern hemisphere, on account of which the average surface temperature over the oceans rises by $\sim$ 1 K by the end of the integration. In addition, it seems that the deep ocean was not in a steady state at the beginning of the control run. The spinup was only 150 years long, whereas the deep ocean might be expected to take several thousand years to reach equilibrium. During the control integration, the deep ocean continues to warm, contributing to sea-level rise. This can be seen by inspection of the depth-profile of fractional expansion at various times during the integration, shown in Figure 1(a), which indicates that the largest effects occur near 1000 m.

We assume that the drift in the control run and the effect of climate change are combined linearly, which is likely to be reasonable since both are small. On this basis, the latter can be obtained by subtracting the control from the anomaly. The depth profile of fractional thermal expansion in (anomaly – control) is presented in Figure 1(b). Unlike the control-run drift, this takes place mostly at the surface, and penetrates to greater depth as the run progresses. This is to be expected, because heat is transported downwards from the surface by turbulent mixing (represented by vertical diffusion in the ocean model) for the most part; it is only in limited regions of the ocean that there is advection of heat directly to considerable depth. Sea-level rise in the control and the anomaly therefore result from different processes, which is a further justification for deducing the signal of climate change by finding the difference between the integrations.

The anomaly run gives a sea-level rise of 213 mm by year 75. The sea-level rise from climate change calculated year by year is shown in Figure 2. It reaches 103 mm by the end of the run. (Note that the two integrations are entirely independent, so the difference series exhibits a greater interannual variability than either of the runs alone.)

Different climate-change experiments employ different greenhouse-gas scenarios and climate sensitivities. Taking these into account, our result for the component of sea-level rise arising from thermal expansion compares well with those from other transient coupled experiments. In particular, the GFDL experiment (IPCC, 1992), with a climate sensitivity of 4·0°C and the same CO_2 scenario as ours, gives a sea-level rise of $\sim$ 170 mm by year 75. Cubasch *et al.* (1992a) report on an experiment conducted at MPI, following IPCC scenario A, in which CO_2 doubles by year 60. In this experiment, which uses a model having a sensitivity of 2·6°C, global-average temperature has risen by $\sim$ 1·7°C by year 75 and sea-level by $\sim$ 80 mm.

3.2 Water balance

As the climate changes, we would be prepared to observe a redistribution of the world's water among its various reservoirs. This could lead to change in the mass of water in the ocean. However, in view of the foregoing discussion, it is clear that we cannot obtain this from the ocean

model itself. The mass of the model ocean is a diagnosed quantity, not a conserved one. Moreover, a small additional non-conservation of mass is implied by the procedures whereby water is exchanged between the atmosphere and ocean models through precipitation and evaporation, while, in the present version of the model, runoff of fresh water from the land into the ocean is not included at all.

For these reasons, in order to diagnose the change of mass of the ocean, which we denote $\Delta(\text{ocean})$, we have to look at the rest of the water balance. In the real world,

$$\Delta(\text{ocean}) = -\Delta(\text{cryosphere} + \text{groundwater} + \text{lakes} + \text{soil moisture} + \text{atmosphere}).$$

Estimates of the equivalent depths of water stored in these various reservoirs are shown in Table 1 (adapted from Brutsaert, 1982). The water balance scheme of the model (the atmosphere model, which includes the land surface) is depicted in Figure 3. Various points must be noted about this:

1. The cryosphere—the area covered by permanent ice-sheets—is represented by a very large depth of lying surface snow. The actual thickness is arbitrary and unrealistic; it is immaterial so long as the ice-sheets are not liable to disappear. The ice-sheets are confined to Antarctica and Greenland; mountain glaciers elsewhere are omitted. As will be discussed below, this omission is a serious shortcoming of the model for our current purposes.

2. Small lakes and rivers are not represented in the model. Large inland seas (namely the Great Lakes and the Caspian and Black Seas) appear and are treated as though they were ocean.

3. The soil moisture content is driven by the flux of (precipitation − evaporation). When the influx exceeds the maximum infiltration rate, "quick" surface runoff is produced. There is also a gravitational drainage, "slow" deep runoff, while the soil is not dry. However, there is no model groundwater reservoir for this to run into.

4. The model includes a "canopy water" reservoir. This is the liquid water which accumulates on vegetation. It is a very small amount and is unimportant for this study, but is included for completeness.

In the model, therefore, we would expect

$$\Delta(\text{ocean}) = -\Delta(\text{snow} + \text{canopy} + \text{soil moisture} + \text{atmosphere}).$$

If the atmosphere model conserves water, we might also expect to be able to compute the change in mass of the ocean by finding the time-integral of the net rate at which water is added to the ocean, which is

$$\text{precipitation over ocean} - \text{evaporation from ocean} + \text{runoff} + \text{calving}.$$

"Calving" is the production of icebergs from the Antarctic and Greenland icesheets; this mechanism returns water from the land to the ocean. Rough figures are given in Table 2 (adapted from Brutsaert, 1982) for the average water fluxes in the global budget. Two points have to be made concerning this approach.

1. Rain (not snow) falling on the ice-sheets always runs off in the model. This is not necessarily realistic. Rain falling far from the coast of Greenland or Antarctica might be expected to freeze or evaporate before it could run off.

2. Calving is not represented in the model. To do so would require a dynamical model of the ice-sheets, which is lacking.

Both of these methods were used to calculate the change in the amount of water in the ocean during the control run using annual means of model quantities. As the water balance should not be shifting, we ought to find zero change of storage in each of the components separately, and we take this to be the case for groundwater and lakes, which are not modelled. However, calving of icebergs is not represented, so an equivalent mass of snow builds up on the ice-sheets and is not returned to the ocean. There is an average accumulation of about 12 cm a^{-1} on Antarctica and about 26 cm a^{-1} on Greenland, which together translate to a sea-level lowering of 6·6 mm a^{-1} as water is permanently removed. (This figure is in line with estimates of accumulation made in or from IPCC (1990) and Fortuin and Oerlemans (1990), for instance.) The land surface model (lying snow, soil and canopy moisture) appears to conserve water accurately. There is an mean water flux (evaporation – precipitation) of 1·6 mm a^{-1} (averaged over the entire globe) into the atmosphere, which does not appear to be balanced by any secular increase in atmospheric water content. Presumably this arises from numerical inaccuracy.

Both methods were also applied to the anomaly integration and, as in the case of thermal expansion, the effect of climate change was found by subtracting the control from the anomaly. Various difficulties concerning this procedure must be discussed.

1. The most serious deficiency is the omission of a model of mountain glaciers outside the areas of permanent ice. It is expected that, on the timescales we are considering, the melting of mountain glaciers would make a contribution to global sea-level rise of a similar magnitude to that from thermal expansion (Meier, 1984; IPCC, 1990, Sections 9.4 and 9.5; Oerlemans and Fortuin, 1992).

2. Since we have no model of the ice-sheets, we have to assume that the rate of calving of icebergs does not change. This is perhaps not unreasonable, since the timescales for significant dynamical changes in the permanent ice-sheets are expected to be long (see, for instance, Fortuin and Oerlemans, 1990). If this assumption is made, the flux due to calving cancels out.

3. As we have observed, the model has no groundwater reservoir. Whereas in the control, we might legitimately suppose that groundwater storage does not change, this is not reasonable for the climate-change experiment. In order to determine what effect there might be on sea-level, we need to know how quickly deep runoff via the groundwater reservoir reaches the ocean, and thus how fast any change in this flux will percolate through the system. The simplest assumptions we could make are either than the timescale is very long compared with the experiment, so that the flux from the groundwater reservoir into the ocean does not change and can be neglected in the difference between the integrations, or that the timescale is short compared with the experiment, so that changes in deep runoff have immediate effect, like those in surface runoff. We choose the latter possibility. Deep and surface runoff are therefore treated together.

4. Without information on where runoff is injected, which we do not have available, we cannot calculate individual water budgets for the inland seas represented in the model geography. We treat them just like ordinary ocean points, assuming they reach a common sea-level with the ocean at large, although this is not really correct if they are not connected to it. The influence of rising or falling water levels in other lakes and rivers is neglected entirely.

5. The non-conservation of water by the atmosphere almost entirely cancels. There is a residual error of $< 0{\cdot}1$ mm a^{-1}. It should be admitted that the calculation is incomplete, in that omits cloud water content—it is based on ambient specific humidity. Cloud water is a relative small part of total atmospheric moisture.

In Figure 4, the time-series of alterations in global-average sea-level caused by changes in storage in the Antarctic and Greenland ice-sheets, snow and soil moisture elsewhere on land, and the atmosphere (neglecting cloud water) are shown separately and in total. By year 75, the difference between the two integrations corresponds to a sea-level rise of 14 mm, seven times

smaller than the part due to thermal expansion (*cf.* also global-average annual precipitation, which is $\sim 1\ \mathrm{m\,a^{-1}}$). A small positive contribution to sea-level rise is made by the average reduction of snowdepth and the drying out of the land surface outside Greenland and Antarctica, and a negative one by increased atmospheric humidity. The largest effect is that of Antarctica. It has been suggested that changes in Antarctica would have a negative effect on sea-level in the short term, since an increase in precipitation there, accompanying rising atmospheric humidity, would outweigh an increase in ablation (melting and sublimation) caused by higher temperatures (*e.g.* Fortuin and Oerlemans, 1990). For roughly the first half of the present experiment, the temperature in Antarctica actually *falls*, leading to the reverse effect, net reductions in the mass of the Antarctic ice-sheet (assuming that the rate of calving is unchanged) until around year 50. The reasons for this are not entirely clear; it is apparently connected with changes in deep mixing in the ocean (see Murphy, 1992). Throughout the experiment, precipitation and runoff (from melting) in Greenland both increase, but the latter rises more rapidly, so that Greenland is also a positive contributor to sea-level. Although the results for Antarctica and Greenland are uncertain on account of our lack of knowledge about future rates of calving, they are consistent with the best estimate of IPCC (1990) in indicating that the effect on sea-level of changes to the ice-sheets will be less on these time scales than that of thermal expansion, despite the fact that the ice-sheets contain a volume of water equivalent to tens of metres of sea-level.

We can address the problem of the lack of mountain glaciers by making an estimate of glacier melt based on IPCC figures obtained from a simple climate model, using their "best estimate" parameters, including a climate sensitivity of 2·5 °C, the same as ours. In the "Business as Usual" scenario the melting of mountain glaciers contributes in the range 20–100 mm to sea-level rise after 45 years (depending on the sensitivity of the glacier mass balance to temperature change). By this time the temperature rise in their model is $\sim 1{\cdot}2\,^{\circ}\mathrm{C}$ (IPCC, 1990, Figure A.9). On a simple proportionality, therefore, we might estimate 30–140 mm as the order of magnitude of sea-level rise from glacier melt from this experiment, several times larger than the contribution from the water balance which can be calculated.

3.3 Total sea-level rise

By combining the calculated results of thermal expansion and changes to the water budget, we arrive at a total of 116 mm for the global-average sea-level rise by year 75 (excluding mountain glaciers). These figures can simply be added because they are both small numbers, compared with the mean ocean depth of $\sim$ 4000 m. The "product" of the two effects, a contribution from the change in density of the additional water, is a negligible second-order term. For this reason also it is unimportant what density we assume the additional water to have, and we take $1000\ \mathrm{kg\,m^{-3}}$ for convenience. The time-series of the total is exhibited in Figure 2.

This cannot be interpreted directly as a prediction, because of the so-called "cold-start" phenomenon (IPCC, 1992), observed also in other transient GCM experiments, that comparatively slow change is observed for the first few decades. This is believed to be an artefact of experimental design, and until it is understood it must not be regarded as legitimate to equate the start of the experiment to the present day or any other particular date. One possible explanation of the effect is that the current climate is not an equilibrium state, because the atmospheric concentrations of greenhouse gases, and hence the radiative forcing of climate, have been changing continuously for perhaps a couple of centuries as a result of industrial emissions. We can attempt to demonstrate this using a simple one-dimensional climate model of the type referred to in the Introduction, a climate sensitivity of 2°C and the same scenario as in the transient experiment for future CO_2 concentrations. We integrate the model (a) from 1765 (taken as the "beginning" of the Industrial Revolution) with estimates of CO_2 emissions since then and (b) from 1990. A cold start lasting about a decade is observed in the modelled temperature series from the latter integration; after this, (b) proceeds similarly to (a) but lagging by about five years. Results such as this from a simple model can only be taken as suggestive of the behaviour of more complex models; the question of the cold start in coupled models is explored in more detail by Hasselmann *et al.* (1992).

4 Local sea-level changes

4.1 Sea-surface topography in the model

The global-average sea-level rise will be locally "modulated" by any changes in relative local sea-surface topography. As has been pointed out already, the Cox ocean model has a rigid lid rather than a free surface. The surface is "kept flat" by the application of a downward rigid-lid pressure $p_s(x, y)$. This pressure may be regarded as the model's equivalent of the sum of two effects, namely the surface atmospheric pressure and the hydrostatic pressure of the "missing" depth of water $h(x, y)$ which would be present if the model had a free surface, *i.e.*

$$p_s = h\rho g + p_a \Rightarrow h = \frac{p_s - p_a}{\rho g}, \tag{3}$$

where g is the acceleration due to gravity and p_a the sea-level atmospheric pressure ($\sim 10^5$ Pa). The rigid-lid pressure p_s is determined by ocean circulation; in this section we show how it may be extracted.

The surface pressure enters the dynamical equations through the pressure gradient term in the equation of motion. In the Cox ocean, the pressure p is replaced by the sum of two terms,

$$p = p_s + g\int_z^0 \rho \, \mathrm{d}z'; \tag{4}$$

the pressure at level z is the sum of the surface pressure, which is transmitted to all depths, and the hydrostatic pressure of the water column between z and the fixed surface. The equation of motion contains a term proportional to $\nabla_H p$, ∇_H being the horizontal gradient operator. Therefore, in view of equation (4), the Cox equation of motion includes the term $\nabla_H p_s$. In the prognostic equations, $\nabla_H p_s$ is eliminated; however, it can be diagnosed from the ocean model output. But since p_s appears only as this gradient, we can obtain p_s and h only to within an arbitrary additive constant (the gradient of a constant vanishes). Hence we cannot obtain absolute sea-surface topography from the model, only relative. This, however, is adequate for the purpose. If we can find the relative changes in local sea-level, and we also know the global-average absolute sea-level rise, the sum of the two will give us the absolute changes in local sea-level.

The method by which p_s is computed is described in more detail in the Appendix. Sea-level atmospheric pressure is obtained from the atmosphere model. The two are combined and converted to a relative topography field h using equation (3) and $\rho g \simeq 1025 \times 9 \cdot 81 \simeq 10^4$ (Pa m^{-1}), which will be correct to within about 1% for the observed range of surface sea-water densities. The calculation is performed for each year of each integration. As an example, in Figure 5 we show p_s, p_a and h averaged over the first 10 years of the control run (*n.b.* dimensionally, p_s and p_a are pressures, h is a distance). The fields have all been adjusted to have zero global average, the datums being arbitrary. In the p_s field, the important features are the strong slope across the Antarctic circumpolar current and the summits at the eyes of the gyres towards the western sides of the Atlantic, Pacific and Indian Oceans, near the Caribbean, Japan and Madagascar respectively. These major features compare qualitatively well with those of the control run of the Hamburg OGCM (Mikolajewicz *et al.*, 1990), and in the Pacific with observations collated by Wyrtki (1974). Variations in p_a are an order of magnitude less than those of p_s, so atmospheric pressure is a less important influence on sea-surface topography. The most obvious feature in this field also is the southern circumpolar vortex; the depression associated with the North Atlantic storm-track, for instance, can also be discerned. The h field has an area-weighted standard deviation of 0·47 m; the highest point is at +0·72 m, off the coast of Japan, the lowest −1·40 m, in the Weddell Sea. There is a height difference of ~ 1 m in all across the southern ocean.

4.2 Relative changes in sea-surface topography

As for global sea-level rise, we calculate the effect of climate change by year y on relative sea-surface topography by finding the difference between control and anomaly integrations from the same year. This is done for changes in rigid-lid and surface atmospheric pressure Δp_s and Δp_a, whence the relative change in surface topography Δh is obtained, all the fields being adjusted to have zero global average, as before. We present results averaged over the last ten years of the experiment, years 66–75. Figures 6 and 7 show Δp_s and Δp_a respectively. The local significance of the observed changes can be assessed by applying t-tests, estimating the annual variance of the p_s and p_a fields from the first ten years of the control run. (It is not possible to use the entire control run to make the estimate because of the climate drift, commented on above.) Maps are presented showing contours of areas of significant change at various confidence levels. A test for a significant change at 90% confidence succeeds over 69% of the ocean area in the case of p_s, and 38% in that of p_a. Overall, there is no significant spatial correlation between the fields.

A map of changes in relative surface topography Δh appears in Figure 8. This field has a standard deviation of 31 mm, an order of magnitude less than the surface topography itself, but comparable to global-average sea-level rise. This justifies our seeking to estimate the local variations. Because variations in Δp_s exceed those in Δp_a by about an order of magnitude, the Δh field is dominated by the effects of changes in ocean circulation. The largest relative sea-level rises, of up to 0·16 m, occur in Baffin Bay and the Davis Strait (between Greenland and Canada), along the east coast of North America and south of Cape Horn. The rise in the western Indian Ocean implied by the Δp_s field is somewhat tempered by the opposite sign of Δp_a there. There is a strong relative fall in sea-level north of the Ross Sea, of 0·14 m at most.

Some features of the relative changes in sea-surface topography are in common with those observed in other simulations with dynamical ocean models. The GFDL coupled experiment (Bryan, K. and W. W. Hsieh, personal communication) also exhibits a strong relative rise off the east coast of North America. It has a marked relative fall in the Weddell Sea and a weaker one north of the Ross Sea: we also see both, but the latter more than the former. Their results show a greater rise in the north Pacific than ours and the patterns in the south Pacific are different. Our results do not bear great similarity to those of the coupled experiment conducted at MPI by Cubasch *et al.* (1992b), but more to that of Mikolajewicz *et al.* (1990), which used the same ocean model, but did not couple it to an atmospheric GCM. They also see considerably raised relative sea-level in the north Atlantic and falls in the Ross Sea. The MPI ocean model, unlike those used by GFDL and ourselves, has a free surface rather than a rigid lid.

4.3 Absolute local sea-level changes

Finally, we add the absolute global-average sea-level rise d, obtained from the calculations of thermal expansion and water budget, to the map of relative changes in sea-surface topography. In principle there could be a contribution to *absolute* sea-level change from changes in atmospheric surface pressure; although its global-average value cannot change if the mass of the atmosphere is constant, the average values over sea and land separately might change. In practice the contribution from this effect is negligible. For years 66–75, the average d = 102 mm. We obtain Figure 9, the absolute changes in local sea-level averaged over the last decade of the experiment. This is positive over more than 99% of the ocean area, but the drop in relative sea-surface topography in the south Pacific is sufficient to outweigh the global-average rise, and a local sea-level fall of 0·04 m results. The largest rises, in the Davis Strait, have a maximum of 0·27 m. Thus, there is a range in sea-level changes of three times the average figure, underlining the importance of considering factors which influence local sea-level, in particular ocean dynamics. This conclusion will hold even if Δh from other models does not agree in detail with our results, which is likely since climate models differ in detail concerning the distribution of surface temperature changes and other relevant quantities.

4.4 Estimating sea-level rise from a sparse network of stations

We can use our results for local absolute sea-level changes to investigate the accuracy of an estimate of global-average sea-level rise derived from a few land-based stations. One approach described by Barnett (1983, 1990) to the estimation of sea-level rise is to identify a small number of key measuring stations, each supposed to be representative of a large geographical area, with their spatial density being proportional to the relative areas of the oceans they sample, in order to achieve an even weighting by sea-area. He lists the ten stations used in one such study, and the nearest model ocean grid-boxes to these stations are shown in black on Figure 8.

An analysis by empiral orthogonal functions (we follow the procedure of Barnett, 1983) is used to search for a spatially coherent signal of sea-level change. When this is done with the annual time-series of relative sea-level at the ten grid-boxes, the strongest signal gives the time-series shown in Figure 10. For the last decade, the mean is 127 mm, which should be compared with the global-average sea-level rise for this decade of 102 mm. The implication is that, if the global average of the model sea-level were calculated from this network of sites, the result for the last decade would be an overestimate by 25%. The uncertainty quoted by Barnett is 10%; however, that figure represents statistical uncertainty, whereas the 25% is a systematic error underlining Barnett's caveat that (at least, on the basis of coastal station data) it is very difficult to extract a reliable result for global sea-level rise, a point reinforced by the observation of Barnett (1984) that variations of up to 50% can result from different choices of methodology alone.

5 Conclusion

This paper has set out an attempt at diagnosing global-average and local changes in sea-level from a coupled ocean–atmosphere climate-change experiment. We have noted various technical difficulties and deficiencies in the model for this purpose, of which the most important is the omission of melting mountain glaciers. Despite its limitations, this exercise serves to illustrate the relative importance of factors which will influence sea-level in the next few decades, particularly thermal expansion, changes in the water budget, and alterations to ocean circulation. However, the time-series of global-average sea-level rise which is presented cannot be interpreted as a prediction for specific future dates because of the cold-start phenomenon, noted in this and other transient GCM experiments. It is clear that global-average sea-level rise, while a useful statistic, is not a sufficient indicator of local sea-level, because local variations are at least as large. Therefore, in this work we have obtained estimates of local mean sea-level changes as well. We have also illustrated the difficulty in determining global sea-level rise from a network of coastal sites, as is generally done in practice, by evaluating an estimate of the global signal from the modelled local sea-level changes at a small number of coastal grid-boxes.

The calculation could be made more complete by incorporating a parameterisation of the melting of mountain glaciers, and possibly also representations of ice-sheet dynamics and the groundwater reservoir, though these are less important. It would of course also benefit from general improvement to climate models; in particular, further investigation is needed into the cold start and the flux corrections. Finally, for studies of the implications of sea-level rise, it would be necessary to investigate extremes in local sea-level (storm surges, for example) as it is these that have the most serious impact.

Acknowledgements

The author would like to acknowledge the assistance and advice of his colleagues James Murphy, Chris Gordon, John Mitchell and Geoff Cookmartin. The cooperation and courtesy of Kirk Bryan and Ulrich Cubasch in providing results and analyses of their own for comparison was greatly appreciated. This work was supported by the UK Department of the Environment under contract PECD 7/12/37.

Appendix

The basic equation of motion for the Cox ocean is

$$\frac{\mathrm{d}\mathbf{u}_H}{\mathrm{d}t} = \frac{\partial \mathbf{u}_H}{\partial t} + \Gamma(\mathbf{u}_H) = -\mathbf{f}\times\mathbf{u}_H + \frac{1}{\rho_0}\mathbf{F} - \frac{1}{\rho_0}\boldsymbol{\nabla}_H p, \tag{5}$$

where $\mathbf{u}_H$ is the horizontal velocity (barotropic + baroclinic), Γ the advection operator ($\Gamma(\mu) = \mathbf{u}\cdot\boldsymbol{\nabla}\mu$ for a scalar μ with $\mathbf{u}$ the 3D velocity), and $\mathbf{f} = f\mathbf{k}$, f being the Coriolis parameter and $\mathbf{k}$ a unit vector in the vertically upward direction. Following the Boussinesq approximation, the density is taken to be a constant reference value $\rho_0 = 1\ \mathrm{g\,cm^{-3}}$ except for the calculation of the horizontal gradient of the pressure p, which has two terms,

$$p(x,y,z) = p_s(x,y) + \int_z^0 g\rho(x,y,z')\,\mathrm{d}z' \Rightarrow \boldsymbol{\nabla}_H p = \boldsymbol{\nabla}_H p_s + \boldsymbol{\sigma},\ \boldsymbol{\sigma} \equiv g\int_z^0 \boldsymbol{\nabla}_H\rho\,\mathrm{d}z'. \tag{6}$$

Note that z is positive upwards and zero at the (fixed) surface, so that in the body of the ocean it is negative. The friction or diffusion term is treated in terms of a viscosity tensor, which is simplified into a constant horizontal part and a stability-dependent vertical part (Pacanowski and Philander, 1981). The surface windstress is applied as a boundary condition to the vertical diffusion term.

Putting together (5) and (6) we obtain

$$\frac{\partial \mathbf{u}_H}{\partial t} = -\Gamma(\mathbf{u}_H) - \mathbf{f}\times\mathbf{u}_H + \frac{1}{\rho_0}\mathbf{F} - \frac{1}{\rho_0}\boldsymbol{\nabla}_H p_s - \frac{1}{\rho_0}\boldsymbol{\sigma},$$

which we then split into two parts thus:

$$\frac{\partial \mathbf{u}_H}{\partial t} = \mathbf{a} - \frac{1}{\rho_0}\boldsymbol{\nabla}_H p_s \tag{7}$$

$$\mathbf{a} = -\Gamma(\mathbf{u}_H) - \mathbf{f}\times\mathbf{u}_H + \frac{1}{\rho_0}\mathbf{F} - \frac{1}{\rho_0}\boldsymbol{\sigma}. \tag{8}$$

Since p_s does not depend on depth, averaging (7) vertically yields

$$\bar{\mathbf{a}} - \frac{1}{\rho_0}\boldsymbol{\nabla}_H p_s = \overline{\frac{\partial \mathbf{u}_H}{\partial t}} = \frac{\partial \bar{\mathbf{u}}_H}{\partial t} = \frac{\partial}{\partial t}\left(\frac{1}{H}\mathbf{k}\times\boldsymbol{\nabla}_H\psi\right) = \frac{1}{H}\,\mathbf{k}\times\boldsymbol{\nabla}_H\frac{\partial\psi}{\partial t}, \tag{9}$$

using the definition of the barotropic stream function ψ. The overline denotes the vertical average

$$\bar{\mu}(x,y) \equiv \frac{1}{H}\int_{-H}^0 \mu(x,y,z)\,\mathrm{d}z.$$

We use (9) in the form

$$\frac{1}{\rho_0}\boldsymbol{\nabla}_H p_s = \bar{\mathbf{a}} - \frac{1}{H}\,\mathbf{k}\times\boldsymbol{\nabla}_H\frac{\partial\psi}{\partial t}, \tag{10}$$

or in components

$$\frac{1}{\rho_0}\frac{\partial p_s}{\partial x} = \bar{a}_x + \frac{1}{H}\frac{\partial^2\psi}{\partial y\,\partial t} \qquad \frac{1}{\rho_0}\frac{\partial p_s}{\partial y} = \bar{a}_y - \frac{1}{H}\frac{\partial^2\psi}{\partial x\,\partial t}.$$

To evaluate $\boldsymbol{\nabla}_H p_s$, we thus need the time derivative of the stream function and the vertical average of (8). The latter requires fields of velocity, temperature T and salinity S (to calculate density) and windstress $\boldsymbol{\tau}$ (for the boundary conditions on $\mathbf{F}$). For the time derivative of the stream function, we use a first-order estimate

$$\frac{\partial\psi}{\partial t} = \frac{\psi(t+\Delta t) - \psi(t)}{\Delta t}.$$

This obtains a field applicable to time $t + \frac{1}{2}\Delta t$, and all other quantities are made consistent with this by taking the means of fields at t and $t + \Delta t$. We use $\Delta t = 1$ a, all fields being annual averages. It is obviously necessary to think about the choice of time interval, because the advection and vertical diffusion terms in (8) are non-linear. However, a test showed that the results obtained by using monthly means and then averaging over the seasonal cycle are not significantly different since it emerges that the linear terms generally dominate, and in any case the variability of the ocean is relatively small (at least on these time scales).

For any scalar ϕ, $\nabla_H \times \nabla_H \phi = \mathbf{0}$. Hence, if $\nabla_H \times \nabla_H p_s$ does not vanish everywhere, we will not be able to find a satisfactory scalar field p_s. In practice, owing to inaccuracy of computation, $\nabla_H p_s$ will indeed not be exactly irrotational. Therefore we use a numerical minimisation to obtain an approximation to p_s and hence h. Obviously, the variations in h must be small compared with the depth; if this were not so, the rigid-lid approximation would not be reasonable. Similarly, differences in surface topography between the integrations must also be small.

This, then, is the means by which h can be extracted from a rigid-lid model. A question to be considered is whether it can in fact be obtained by any more direct means from the density structure of the ocean, without needing a numerical minimisation. We may write (10) and (8) roughly in words as

$$\nabla_H p_s = \bar{\mathbf{a}} - \text{barotropic} = -\text{advection} + \text{Coriolis} + \text{diffusion} - \text{hydrostatic} - \text{barotropic}.$$

Therefore the net pressure gradient

$$\nabla_H p = \nabla_H p_s + \text{hydrostatic} = -\text{advection} + \text{Coriolis} + \text{diffusion} - \text{barotropic}. \tag{11}$$

The depth-average $\bar{\sigma}$ of the Cox hydrostatic term is the dominant contribution to $\bar{\mathbf{a}}$, which itself is much larger than the barotropic part. Hence we expect that the RHS of (11) to be small compared with either of the terms in the middle member, which will be of similar size and opposite sign, *i.e.* $\bar{\sigma}$ more or less balances $\nabla_H p_s$, which we take as representing the surface topography. The largest term on the RHS is the Coriolis effect, *i.e.* the geostrophic approximation holds, in which $\nabla_H p$ is balanced by the Coriolis term, except near the surface, where the Ekman balance obtains.

If we set the RHS to zero, we have

$$\nabla_H p_s = -\bar{\sigma} = -\frac{1}{H}\int_{-H}^{0} \sigma \, \mathrm{d}z = -\frac{g}{H}\int_{-H}^{0}\int_{z}^{0} \nabla_H \rho \, \mathrm{d}z' \, \mathrm{d}z. \tag{12}$$

From $\nabla_H p_s$ we obtain h. (12) is telling us that $\nabla_H p_s$ is determined by $\bar{\sigma}$. Is $\bar{\sigma}$ significantly different from

$$\nabla_H \bar{p} = g \nabla_H \left\{ \frac{1}{H}\int_{-H}^{0}\int_{z}^{0} \rho \, \mathrm{d}z' \, \mathrm{d}z \right\},$$

the gradient of the depth-average hydrostatic pressure (*cf.* depth-average of the hydrostatic pressure gradient)? If $\bar{\sigma}$ could be replaced by $\nabla_H \bar{p}$, (12) would become $\nabla_H p_s = -\nabla_H \bar{p}$, *i.e.* we would have that $\nabla_H p_s$ equals the gradient of a scalar, and hence we would know p_s (to within a constant) immediately, without having to perform the numerical inversion. Operating with ∇_H on the expression in braces,

$$\nabla_H \bar{p} = -\frac{g}{H}(\nabla_H H)\bar{p} + \frac{g}{H}(\nabla_H H)\int_{-H}^{0} \rho \, \mathrm{d}z + \bar{\sigma}. \tag{13}$$

The first two terms contain the quantity $(\nabla_H H)/H$ multiplying, respectively, the depth-average and the bottom hydrostatic pressure, which might be expected to be of the same order of magnitude and different by a factor of around two (since density is roughly constant). $(\nabla_H H)/H$ is the effect of bottom topography, which is a field of steep gradients and large plateaux, and it turns out that the sum of the first two terms is about 10^4 times larger than the third term. $\nabla_H \bar{p}$

is therefore practically completely determined by bottom topography, rather than the surface topography through $\nabla_H p_s$. Thus, we cannot avoid the numerical inversion of p_s in order to obtain the surface topography.

Now we turn to the difference between experiments. The formulae are the same, with the replacement of pressures and densities by differences, since the terms we are concerned with are all linear. Hence, corresponding to (13),

$$\Delta\nabla_H\bar{p} = -\frac{g}{H}(\nabla_H H)\Delta\bar{p} + \frac{g}{H}(\nabla_H H)\int_{-H}^{0}\Delta\rho\,\mathrm{d}z + \frac{g}{H}\int_{-H}^{0}\int_{z}^{0}\Delta\nabla_H\rho\,\mathrm{d}z'\,\mathrm{d}z.$$

There is a crucial difference in this case, however, in that the density changes are mostly restricted to a layer near to the surface. Therefore the first and second terms, respectively proportional to the depth-average and bottom *change* in hydrostatic pressure, are of nearly equal size, since most of the water column experiences the effect of changes near to the surface. Thus these terms tend to cancel each other. In fact, a detailed calculation makes the average magnitude of their sum about five times smaller than that of the third term, which is itself about three times smaller than the average $|\bar{\sigma}|$ in the control run—this is as expected, because we noted that the range of h is greater than that of Δh by a similar factor. Hence, in the difference between initial and final climates,

$$\Delta\nabla_H\bar{p} \simeq \frac{g}{H}\int_{-H}^{0}\int_{z}^{0}\Delta\nabla_H\rho\,\mathrm{d}z'\,\mathrm{d}z = \Delta\bar{\sigma} = -\Delta\nabla_H p_s,$$

using (12), where we assume that only the hydrostatic term is of significance in the equations of motion. Therefore

$$\Delta\bar{p} = -\Delta p_s + \text{const} = -g\rho\Delta h + \text{const},$$

i.e. we can obtain the change in surface topography directly from the change in density structure.

Now

$$\Delta\bar{p} = g\Delta\left\{\frac{1}{H}\int_{-H}^{0}\int_{z}^{0}\rho\,\mathrm{d}z'\,\mathrm{d}z\right\} \simeq g\int_{-H}^{0}\Delta\rho\,\mathrm{d}z$$

if the density changes are near to the surface, just as above, because throughout the majority of the water column, and hence in the depth-average, the entire change in hydrostatic pressure is experienced. Then by combining the last two equations we find that

$$\rho\Delta h \simeq -\int_{-H}^{0}\Delta\rho\,\mathrm{d}z + \text{const}.$$

Since ρ is nearly constant,

$$\Delta h + \text{const}. \simeq -\int_{-H}^{0}\frac{\Delta\rho}{\rho}\,\mathrm{d}z \equiv \Delta\eta.$$

This quantity appeared in equation 2; its area-average is the global-average sea-level rise if there are no salinity changes. It gives a good estimate of the changes in local relative topography, without the need for the numerical minimisation, provided that the hydrostatic pressure is the dominant term in the equation of motion (which it is), and that the changes in density are restricted to a shallow layer. If the latter is the case, we can further replace $H(x,y)$ with a constant (and sufficiently large) H_0, and note that

$$\Delta\eta_0 = -\int_{-H_0}^{0}\frac{\Delta\rho}{\rho}\,\mathrm{d}z$$

is in fact the change in dynamic topography relative to H_0 as a "level of no motion".

Calculating $\Delta\eta$ (and subtracting its area-average), we observe that it is mostly similar to Δh (which is computed with zero area-average). However, the two quantities are not identical,

and substantial differences do arise in some places. The largest, of over 50 mm in magnitude, occur in the areas of greatest change in local topography, namely west of Greenland and north of the Ross Sea, two regions in which changes in temperature penetrate to considerable depth. It should be emphasised that $\Delta\eta$ is not the result of simply imposing a warming in the ocean, in the manner of Church *et al.* Since it is diagnosed from the ocean model, it represents a temperature structure which is dynamically determined.

References

Barnett, T. P., 1983: Possible changes in global sea level and their causes. *Clim. Change*, **5**, 15–38.

—, **1984:** The estimation of "global" sea level change; a problem of uniqueness. *J. Geophys. Res.*, **89**, 7980–7988.

—, **1990:** Recent changes in sea level: a summary. *Sea-level change.* National Research Council, Washington DC

Brutsaert, W., 1982: *Evaporation into the atmosphere.* Kluwer Academic Publishers.

Church, J. A., J. S. Godfrey, D. R. Jackett and T. J. McDougall, 1991: A model of sea level rise caused by ocean thermal expansion. *J. Climate*, **4**, 438–456.

Cox, M. D., 1984: *A primitive equation, three dimensional model of the ocean.* GFDL Ocean Group Technical Report No. 1, GFDL, Princeton.

Cubasch, U., K. Hasselmann, H. Höck, E. Maier-Reimer, U. Mikolajewicz, B. D. Santer and R. Sausen, 1992a: Time-dependent greenhouse warming computations with a coupled ocean–atmosphere model. *Clim. Dyn.*, **8**, 55–69.

Cubasch, U., B. D. Santer, A. Hellbach, G. Hegerl, H. Höck, E. Maier-Reimer, U. Mikolajewicz, A. Stössel, R. Voss, 1992b: *Monte-Carlo climate change forecasts with a global coupled ocean–atmosphere model.* Max-Planck-Institut für Meteorologie Report No. 97, MPI, Hamburg.

Fortuin, J. P. F. and J. Oerlemans, 1990: Parameterization of the annual surface temperature and mass balance of Antarctica. *Ann. Glaciol.*, **14**, 78–84.

Gregory, D. and P. R. Rowntree, 1990: A mass-flux convection scheme with representation of cloud ensemble characteristics and stability dependent closure. *Mon. Wea. Rev.*, **118**, 1483–1506.

Hasselmann, K., R. Saussen, E. Maier-Reimer and R. Voss, 1992: *On the cold start problem in transient simulations with coupled ocean–atmosphere models.* Max-Planck-Institut für Meteorologie Report No. 83, MPI, Hamburg.

IPCC, 1990: *Climate change: the IPCC scientific assessment.* J. T. Houghton, G. J. Jenkins and J. J. Ephraums, Eds., Cambridge University Press.

IPCC, 1992: *Climate change 1992: the supplementary report to the IPCC scientific assessment.* J. T. Houghton, B. A. Callander and S. K. Varney, Eds., Cambridge University Press.

Kraus, E. B. and J. S. Turner, 1967: A one dimensional model of the seasonal thermocline. Part II. *Tellus*, **19**, 98–105.

Meier, M. F., 1984: Contribution of small glaciers to global sea-level. *Science*, **226**, 1418–1421.

Mikolajewicz, U., B. D. Santer and E. Maier-Reimer, 1990: Ocean response to greenhouse warming. *Nature*, **345**, 589–593.

Murphy, J. M., 1992: *A prediction of the transient response of climate.* Meteorological Office Climate Research Technical Note 32, UK Meteorological Office, Bracknell.

Oerlemans, J. and J. P. F. Fortuin, 1992: Sensitivity of glaciers and small ice caps to greenhouse warming. *Science*, **258**, 115–117.

Pacanowski, R. C. and S. G. Philander, 1981: Parametrization of vertical mixing in numerical models of tropical oceans. *J. Phys. Oceanogr.*, **11**, 1443–1451.

Palmer, T. N., G. J. Shutts and R. Swinbank, 1986: Alleviation of a systematic westerly bias in general circulation and numerical weather prediction models through an orographic gravity wave drag parametrization. *Quart. J. Roy. Met. Soc.*, **112**, 1001–1039.

Redi, M. H., 1982: Oceanic isopycnal mixing by coordinate rotation. *J. Phys. Oceanogr.*, **12**, 1154–1158.

Semtner, A. J., 1976: A model for the thermodynamic growth of sea ice in numerical investigations of climate. *J. Phys. Oceanogr.*, **6**, 379–389.

Smith, R. N. B., 1990: A scheme for predicting layer clouds and their water content in a general circulation model. *Quart. J. Roy. Met. Soc.*, **116**, 435–460.

Warrilow, D. A. and E. Buckley, 1989: The impact of land surface processes on the moisture budget of a climate model. *Ann. Geophysicæ*, **7**, 439–450.

Wigley, T. M. L. and S. C. B. Raper, 1987: Thermal expansion of sea water associated with global warming. *Nature*, **330**, 127–131.

Tables

Table 1: Global water storage

Reservoir	Depth/m
Oceans	2600
Cryosphere	50
Groundwater	50
Lakes	0.3
Soil moisture	0.1
Atmosphere	0.025

Approximate figures, averaged over the global surface area.

Table 2: Water fluxes

	Flux/m a^{-1}
Precipitation over land P_L	0.2
Evaporation over land E_L	0.1
Precipitation over oceans P_O	0.8
Evaporation over oceans E_O	0.9
Runoff Y	0.1
Calving C	0.005

Approximate figures, averaged over the global surface area. The same symbols are used to label the fluxes in Figure 3.

Figure captions

Figure 1: Vertical profiles of thermal expansion of sea-water

Fractional expansion w.r.t. year 1 of various years (a) control run; (b) anomaly run

Figure 2: Time-series of global-average sea-level changes

Figure 3: Model water balance scheme

P, E are fluxes of precipitation and evaporation; C is the calving of icebergs. Calving and the groundwater reservoir are not represented in the model, and shown as dotted in this diagram. Approximate figures for the storage in the reservoirs and the fluxes between them can be found in Tables 1 and 2.

Figure 4: Time-series of changes in components of the water balance

Figure 5: Sea-surface topography, years 1–10 of the control run

(a) Rigid-lid pressure p_s; (b) Relative surface atmospheric pressure p_a; (c) Sea-surface topography h

Figure 6: Changes Δp_s in rigid-lid pressure, years 66–75 of the experiment

(a) Δp_s; (b) lower tail probability of a t-test, using years 1–10 of the control run to estimate the variance

Figure 7: Changes Δp_a in surface atmospheric pressure, years 66–75 of the experiment

(a) Δp_a; (b) lower tail probability of a t-test, using years 1–10 of the control run to estimate the variance

Figure 8: Relative changes Δh in sea-surface topography, years 66–75

The ten grid-boxes shown in black are the set used to estimate the global sea-level rise by the method of Barnett (1983).

Figure 9: Absolute changes $d + \Delta h$ in sea-surface topography, years 66–75

Figure 10: Time-series of model global sea-level rise derived from ten coastal grid-boxes

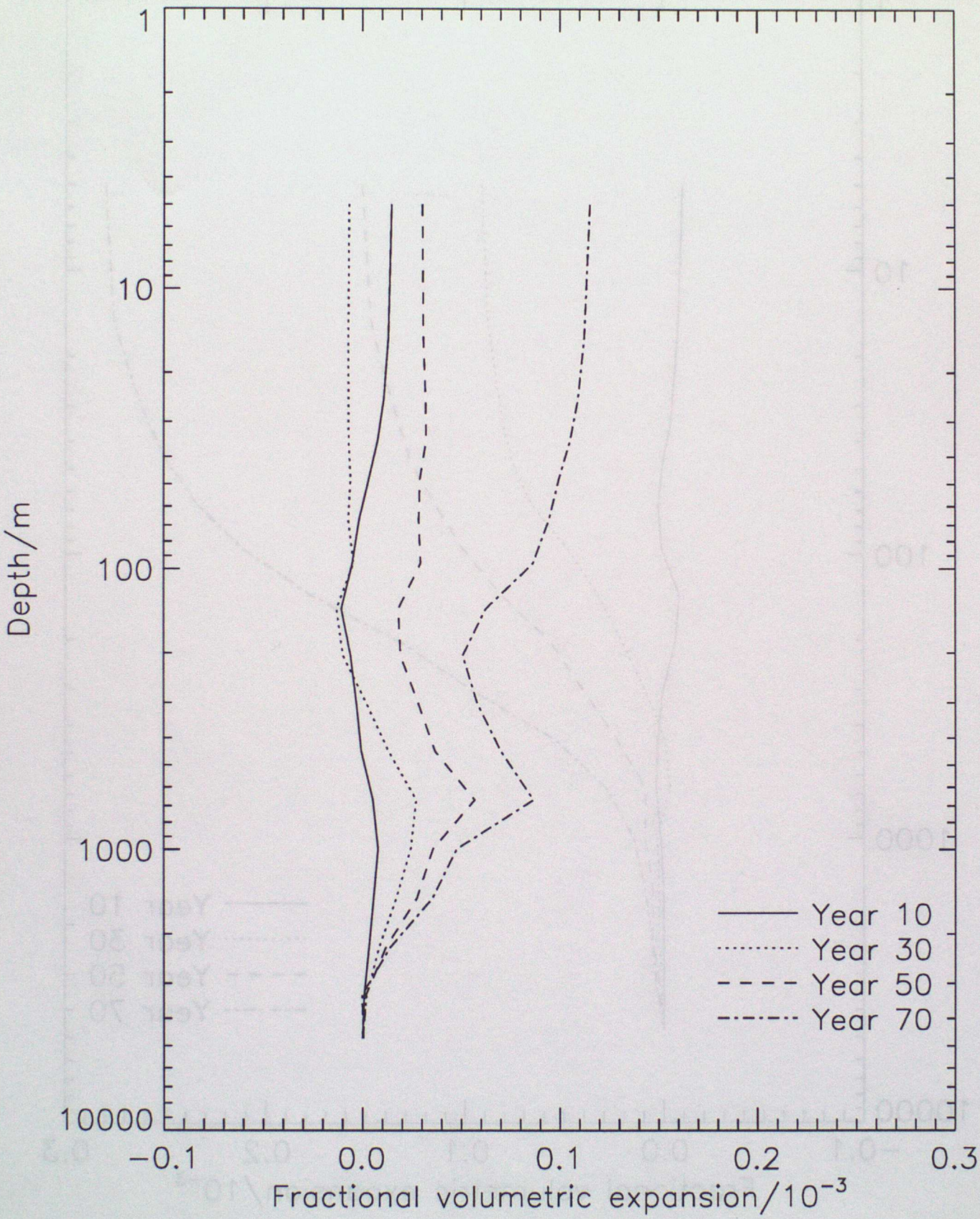
1
10
100
1000
10000
Depth/m
−0.1
0.0
0.1
0.2
0.3
Fractional volumetric expansion/10^{-3}
Year 10
Year 30
Year 50
Year 70

Figure 1a

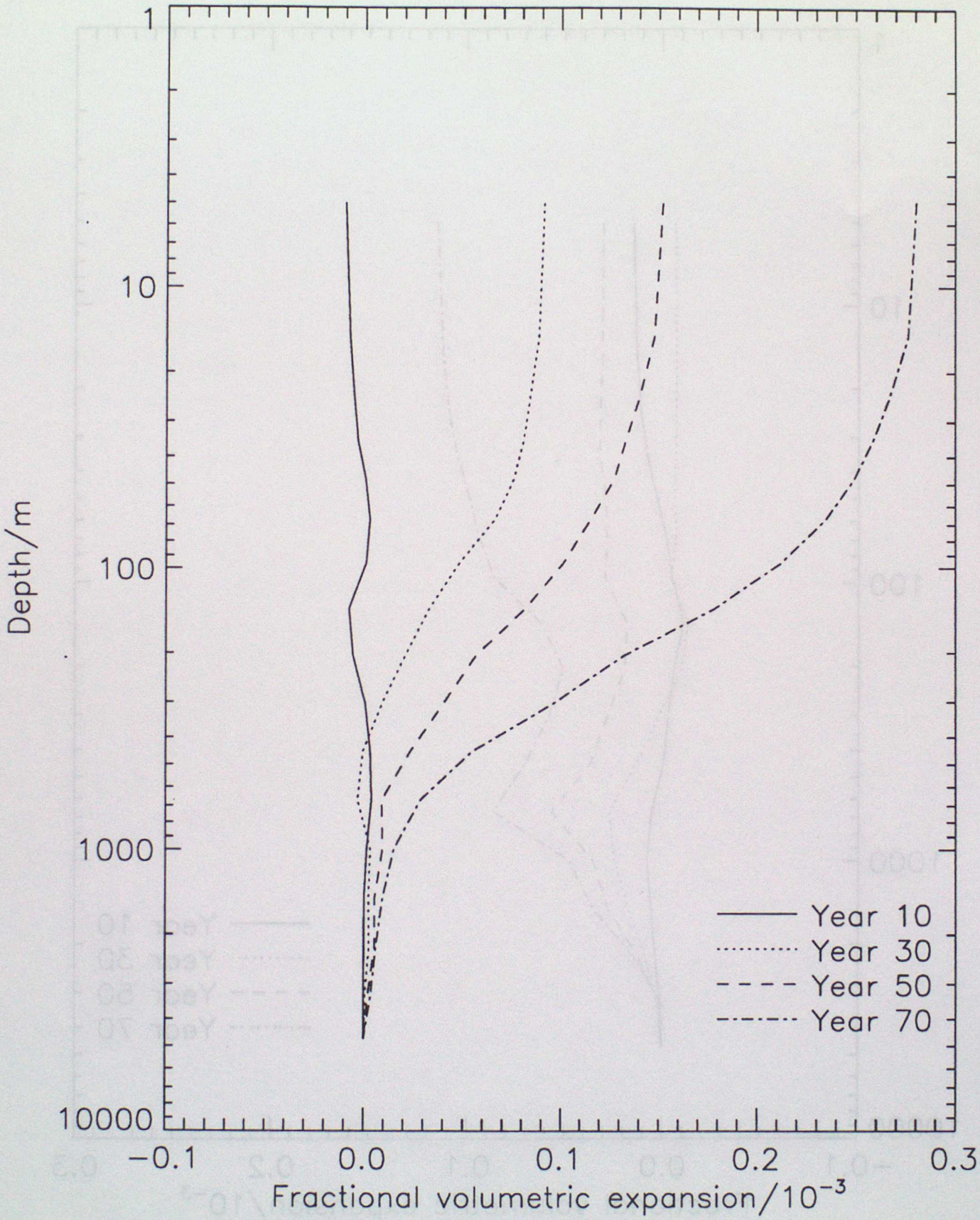
1
10
100
1000
10000
Depth/m
−0.1
0.0
0.1
0.2
0.3
Fractional volumetric expansion/10^{-3}
Year 10
Year 30
Year 50
Year 70

Figure 1b

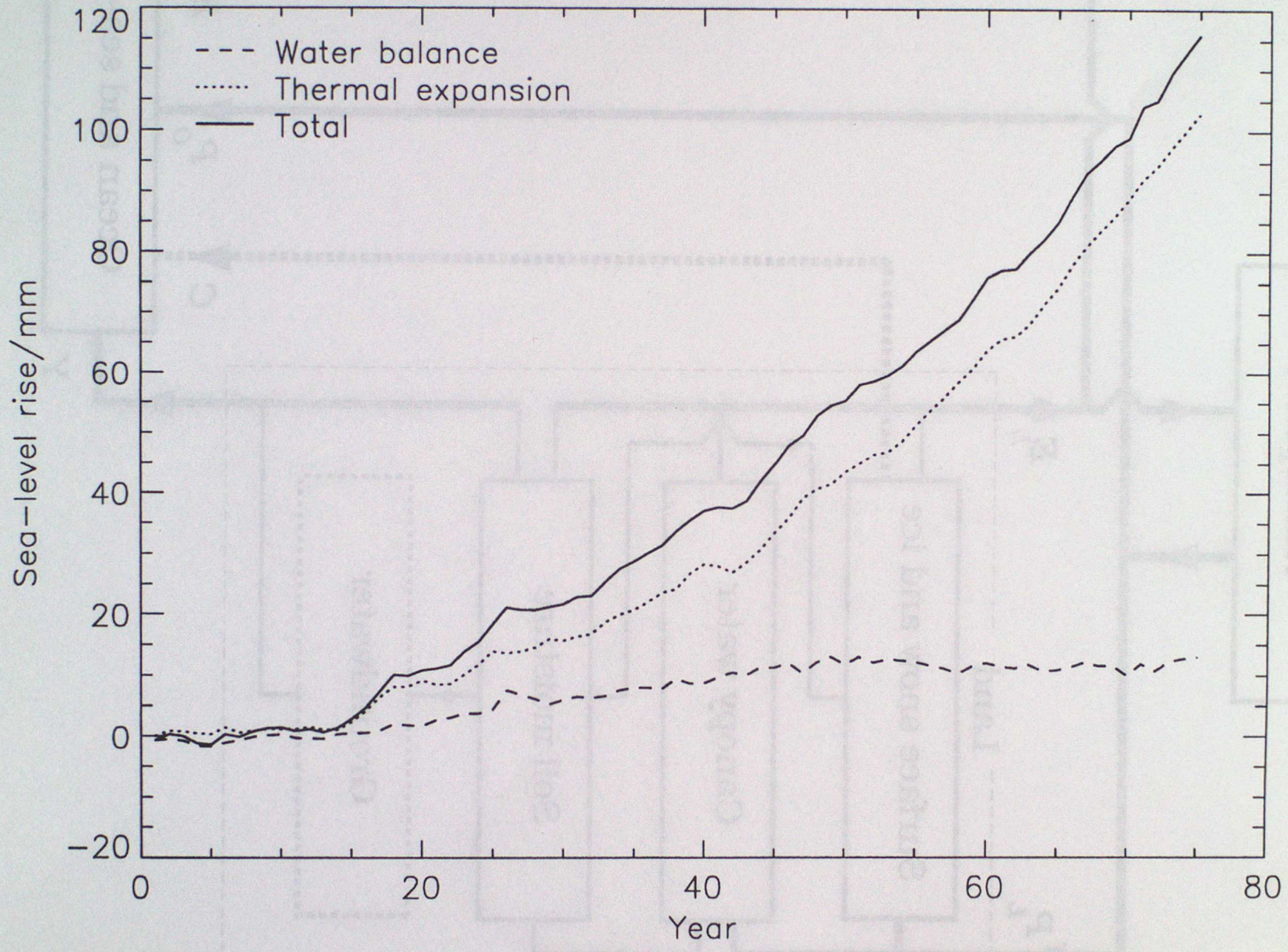
Water balance
Thermal expansion
Total
Sea-level rise/mm
120
100
80
60
40
20
0
-20
0
20
40
60
80
Year

Figure 2

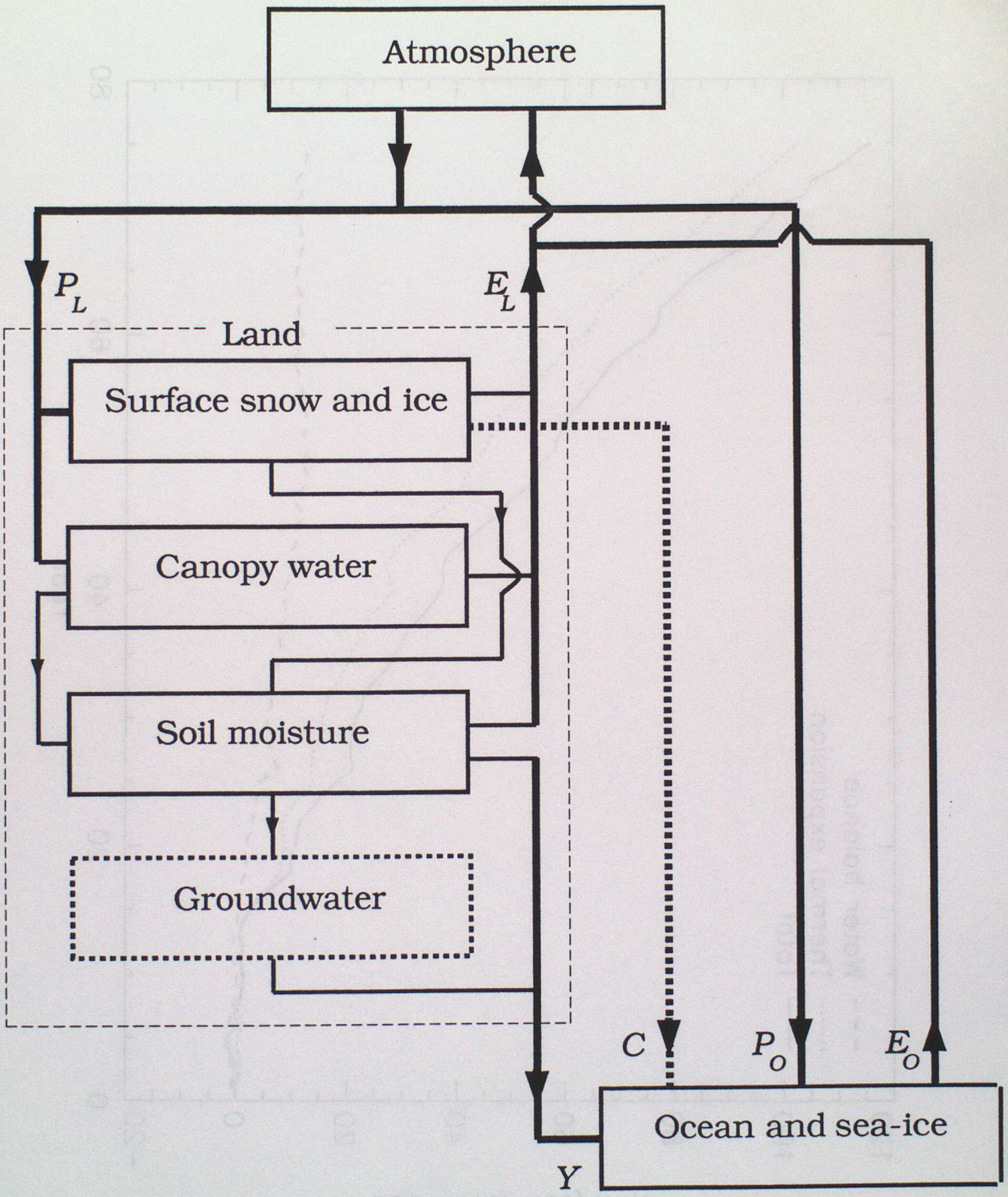
Atmosphere
P_L
E_L
Land
Surface snow and ice
Canopy water
Soil moisture
Groundwater
C
P_O
E_O
Ocean and sea-ice
Y

Figure 3

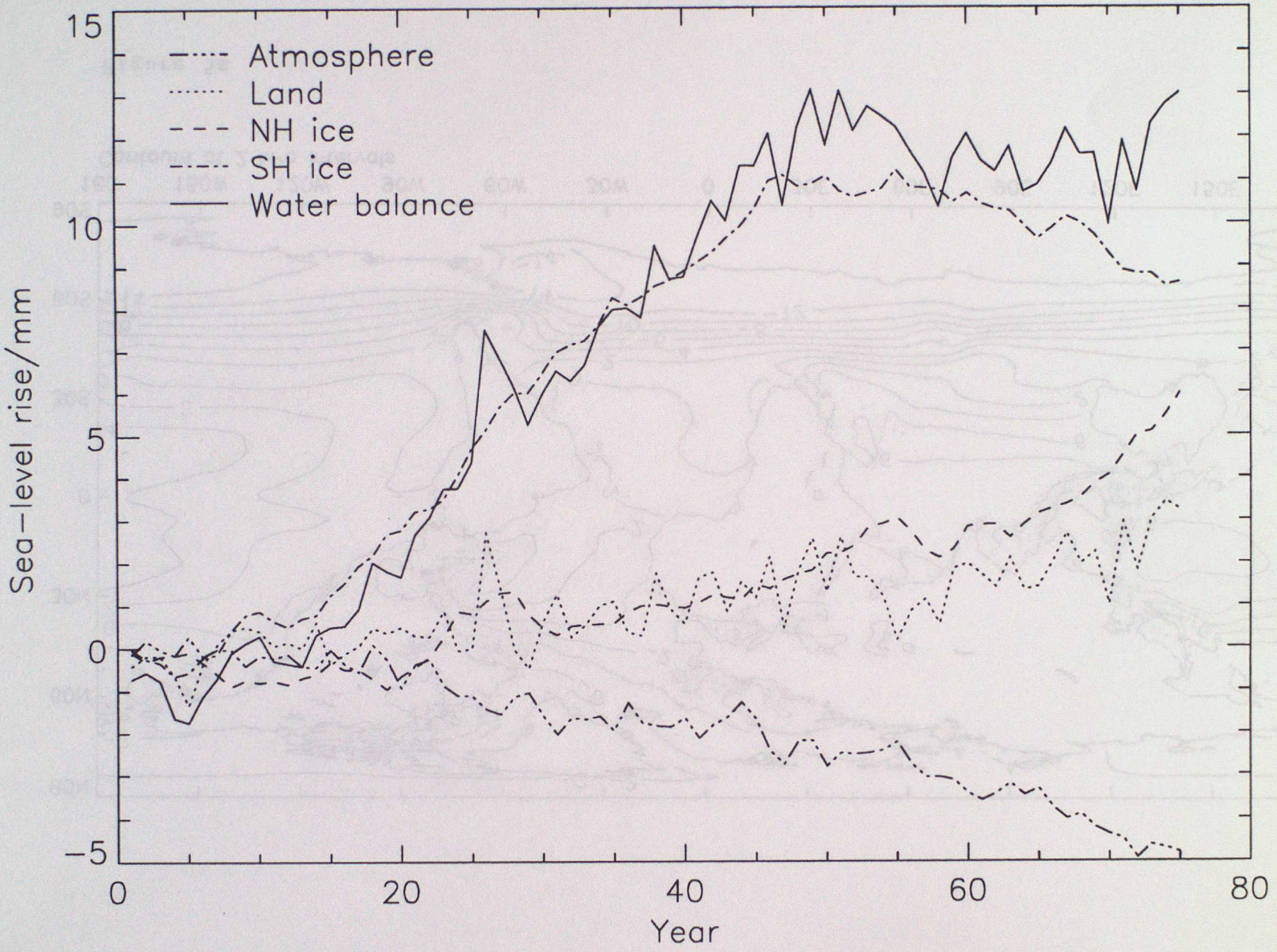
Atmosphere
Land
NH ice
SH ice
Water balance
Sea–level rise/mm
Year
15
10
5
0
−5
0
20
40
60
80

Figure 4

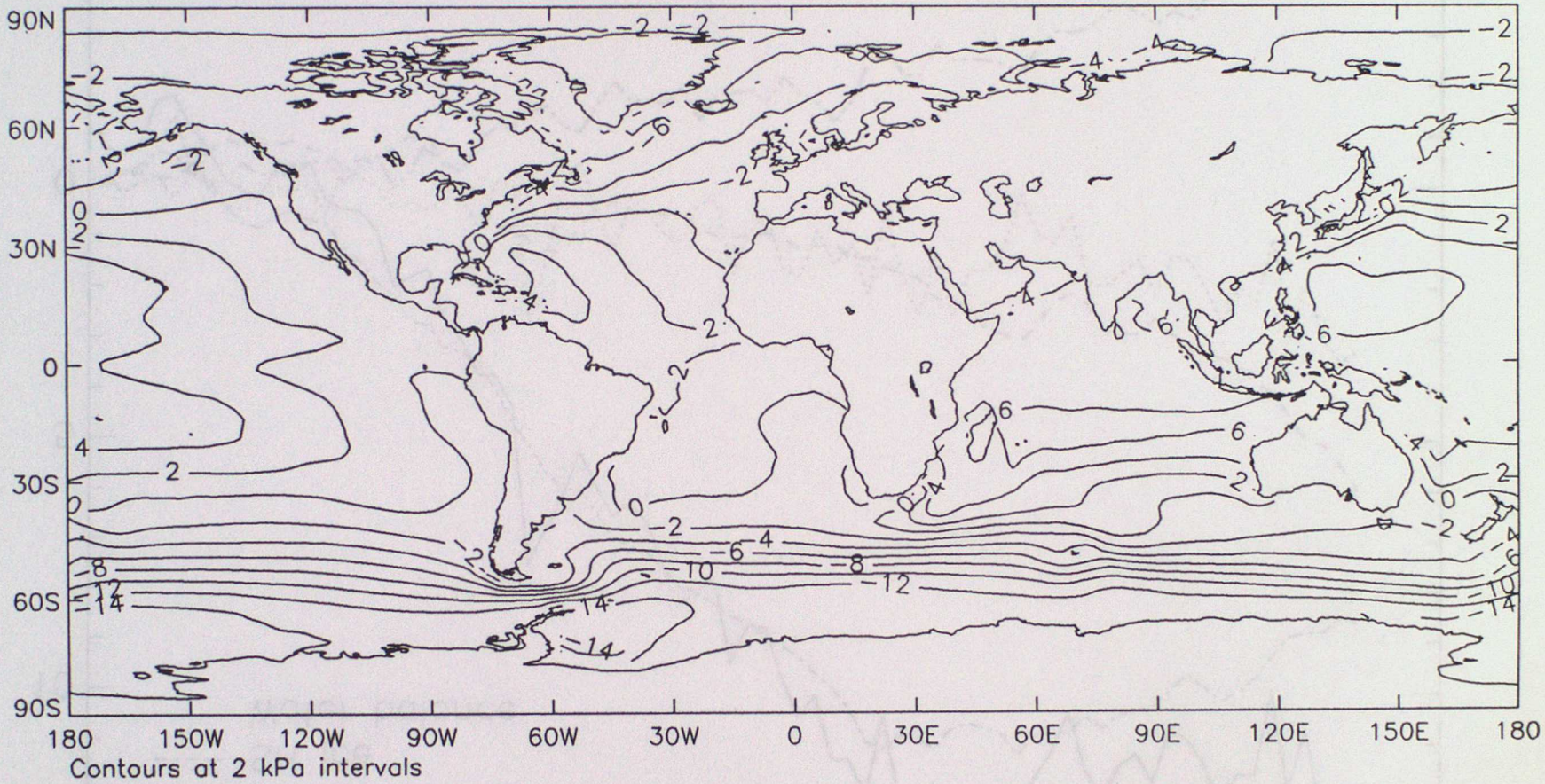
90N
60N
30N
0
30S
60S
90S
180
150W
120W
90W
60W
30W
0
30E
60E
90E
120E
150E
180
Contours at 2 kPa intervals

Figure 5a

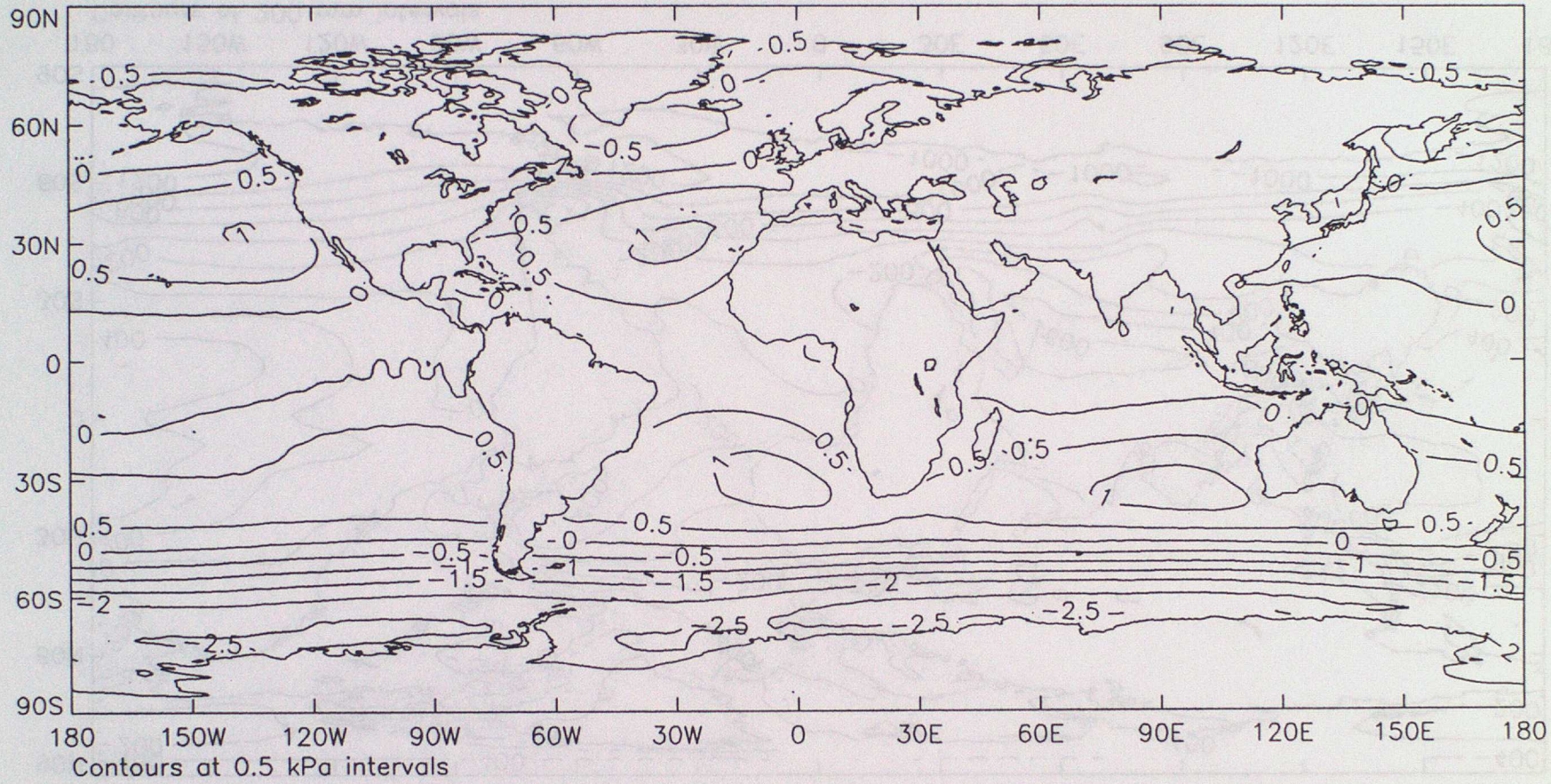
90N
60N
30N
0
30S
60S
90S
180
150W
120W
90W
60W
30W
0
30E
60E
90E
120E
150E
180
Contours at 0.5 kPa intervals

Figure 5b

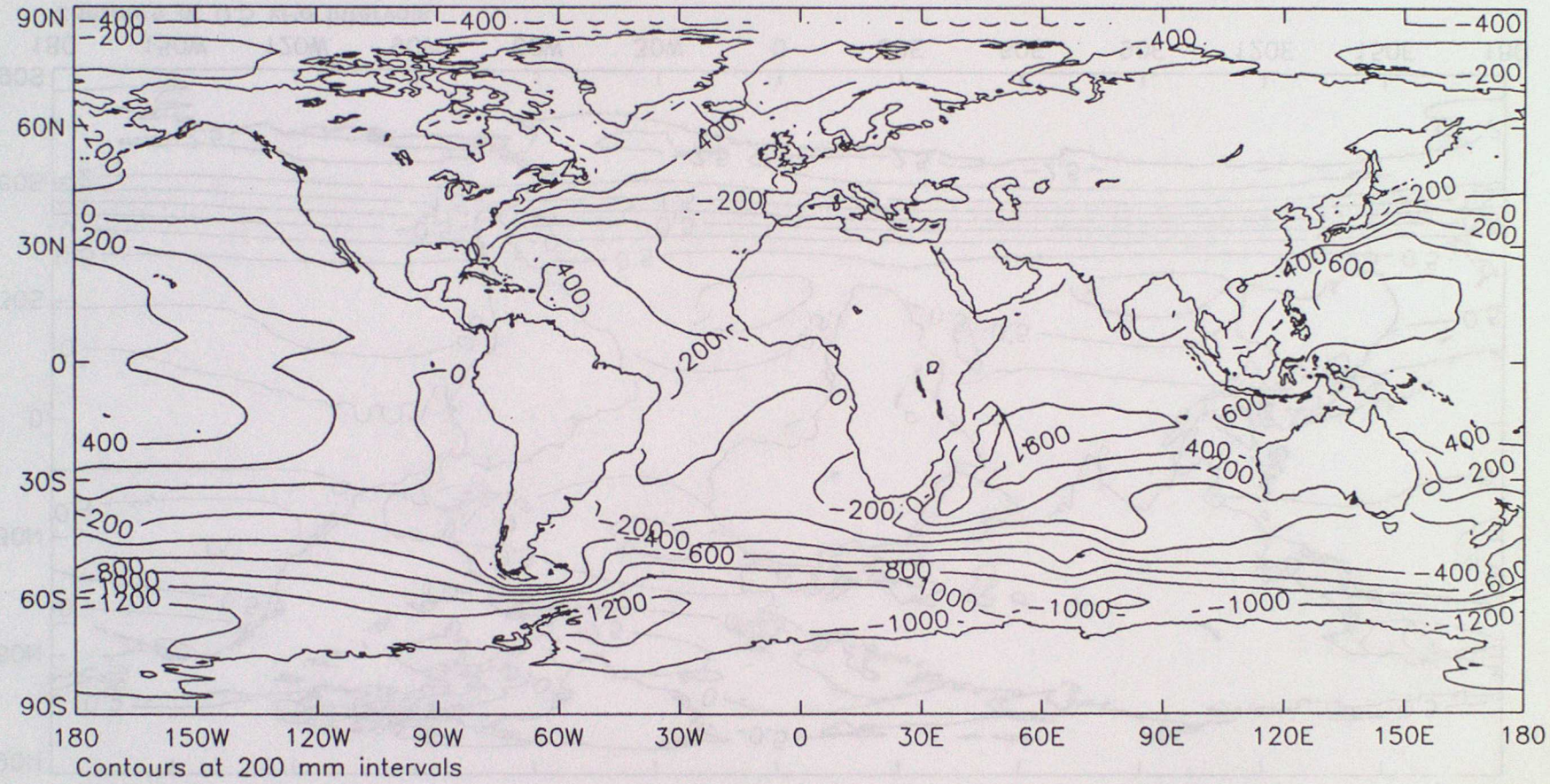
90N
60N
30N
0
30S
60S
90S
180
150W
120W
90W
60W
30W
0
30E
60E
90E
120E
150E
180
Contours at 200 mm intervals

Figure 5c

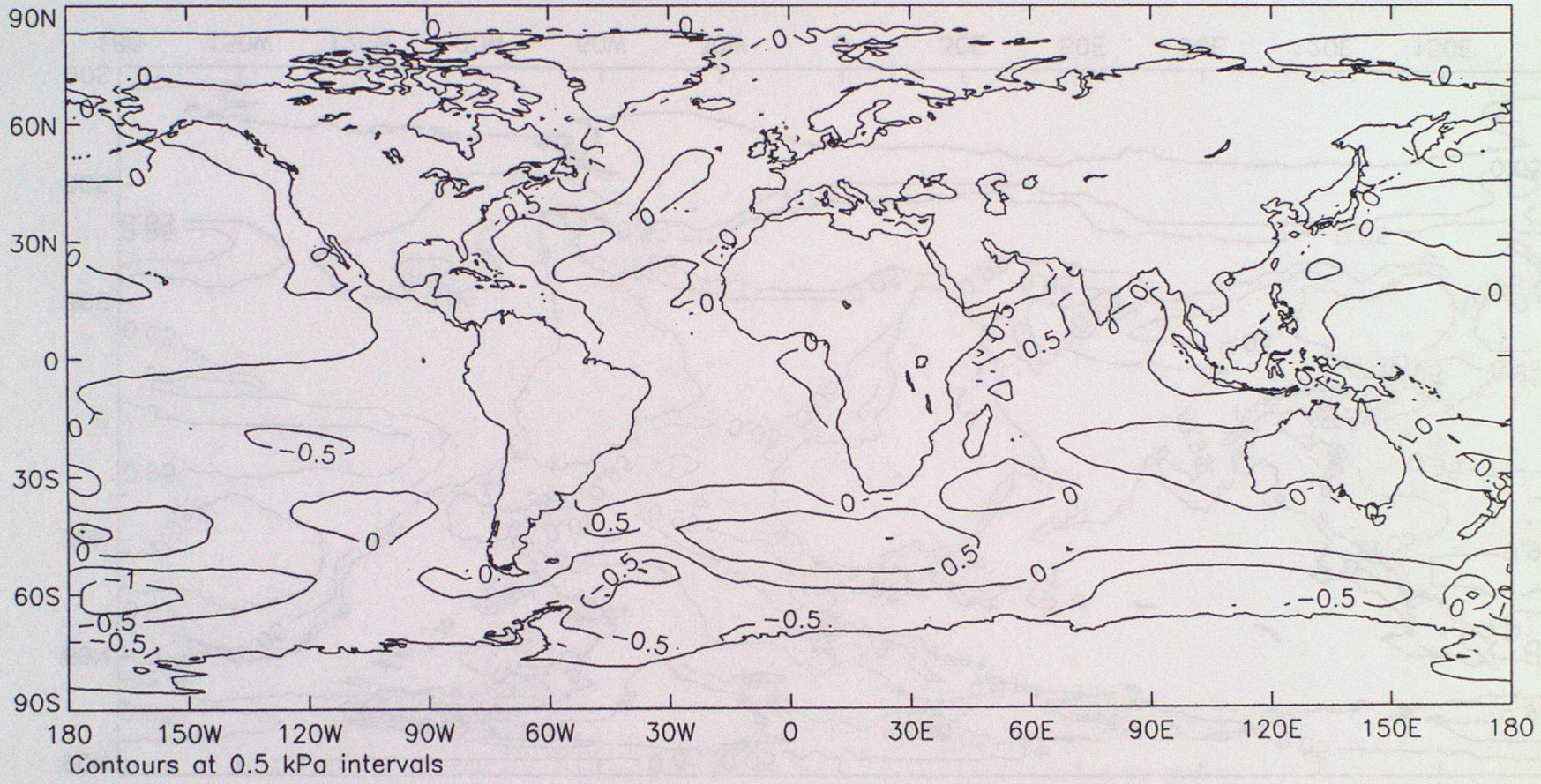
90N
60N
30N
0
30S
60S
90S
180
150W
120W
90W
60W
30W
0
30E
60E
90E
120E
150E
180
Contours at 0.5 kPa intervals

Figure 6a

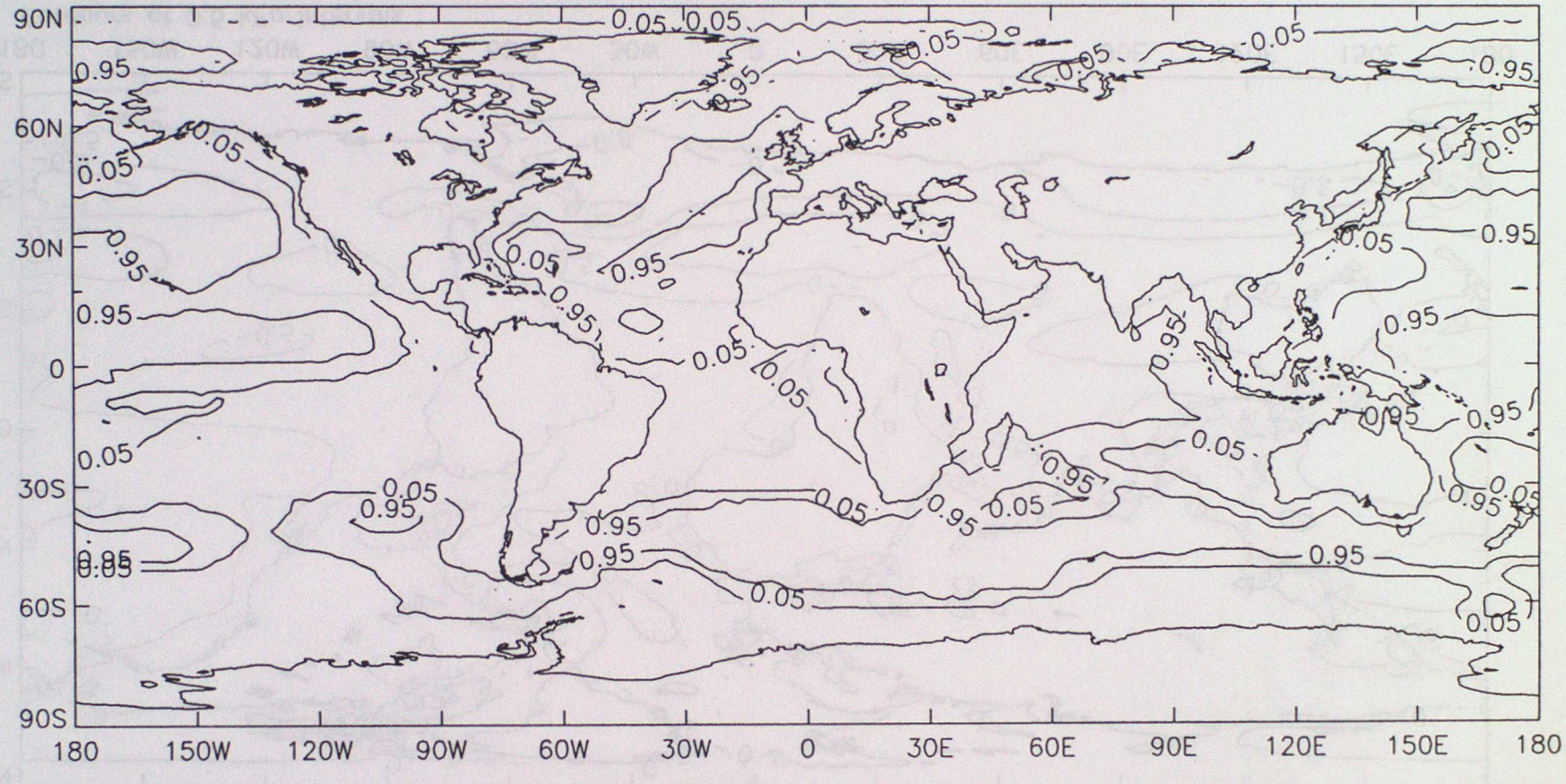
90N
60N
30N
0
30S
60S
90S
180
150W
120W
90W
60W
30W
0
30E
60E
90E
120E
150E
180
0.05
0.95

Figure 6b

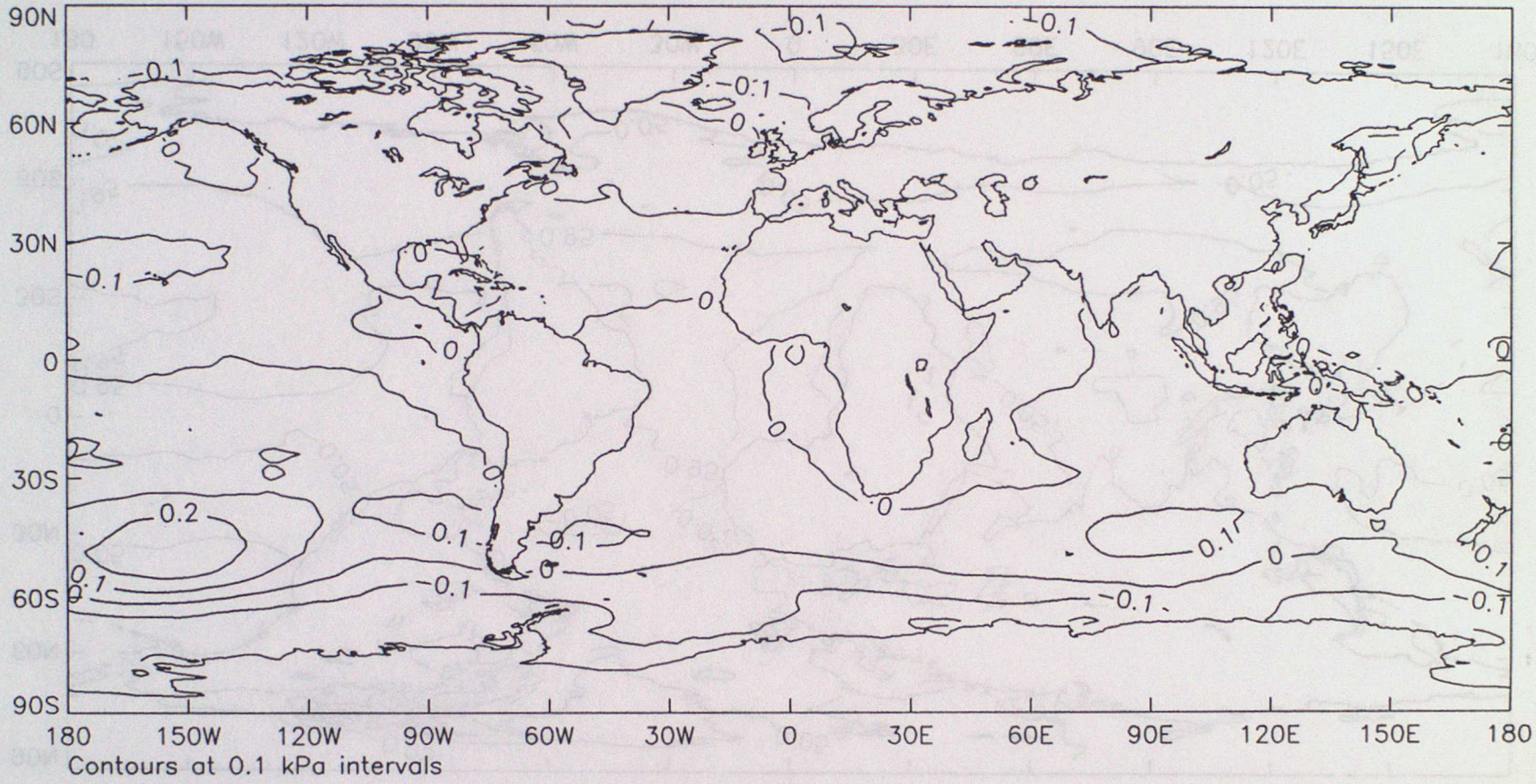
90N
60N
30N
0
30S
60S
90S
180
150W
120W
90W
60W
30W
0
30E
60E
90E
120E
150E
180
Contours at 0.1 kPa intervals

Figure 7a

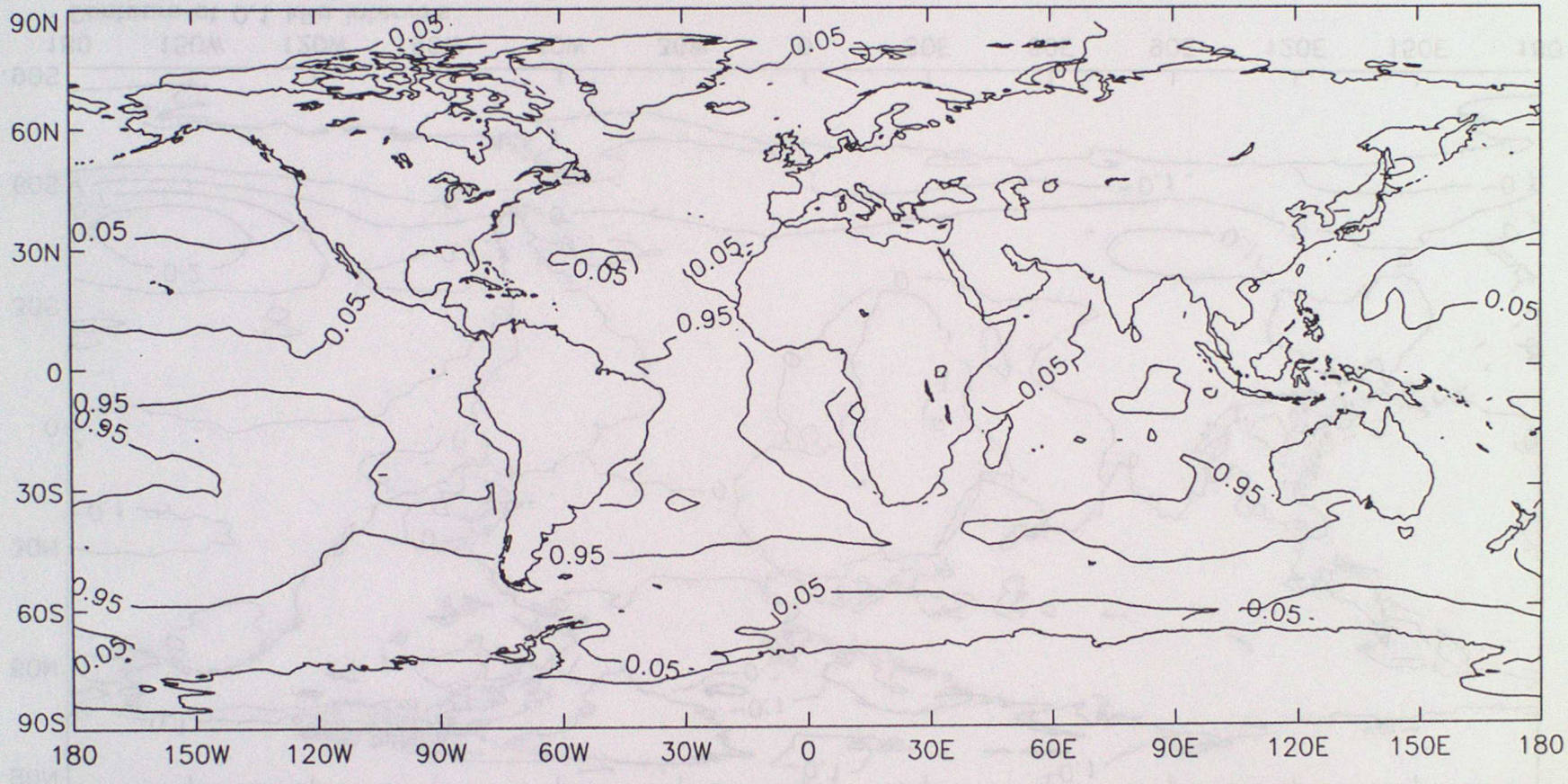
90N
60N
30N
0
30S
60S
90S
180
150W
120W
90W
60W
30W
0
30E
60E
90E
120E
150E
180
0.05
0.95

Figure 7b

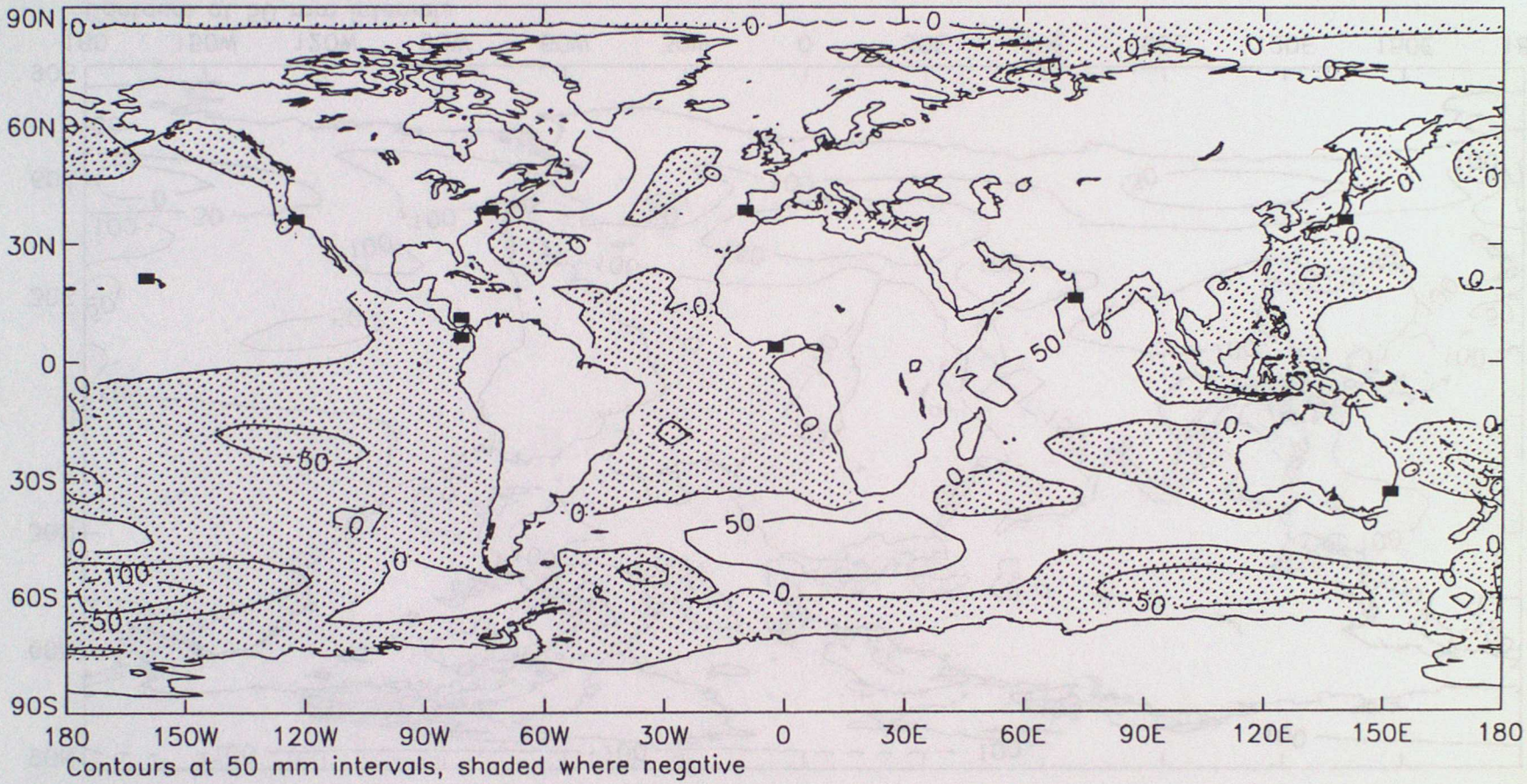
90N
60N
30N
0
30S
60S
90S
180
150W
120W
90W
60W
30W
0
30E
60E
90E
120E
150E
180
0
50
-50
-100
Contours at 50 mm intervals, shaded where negative

Figure 8

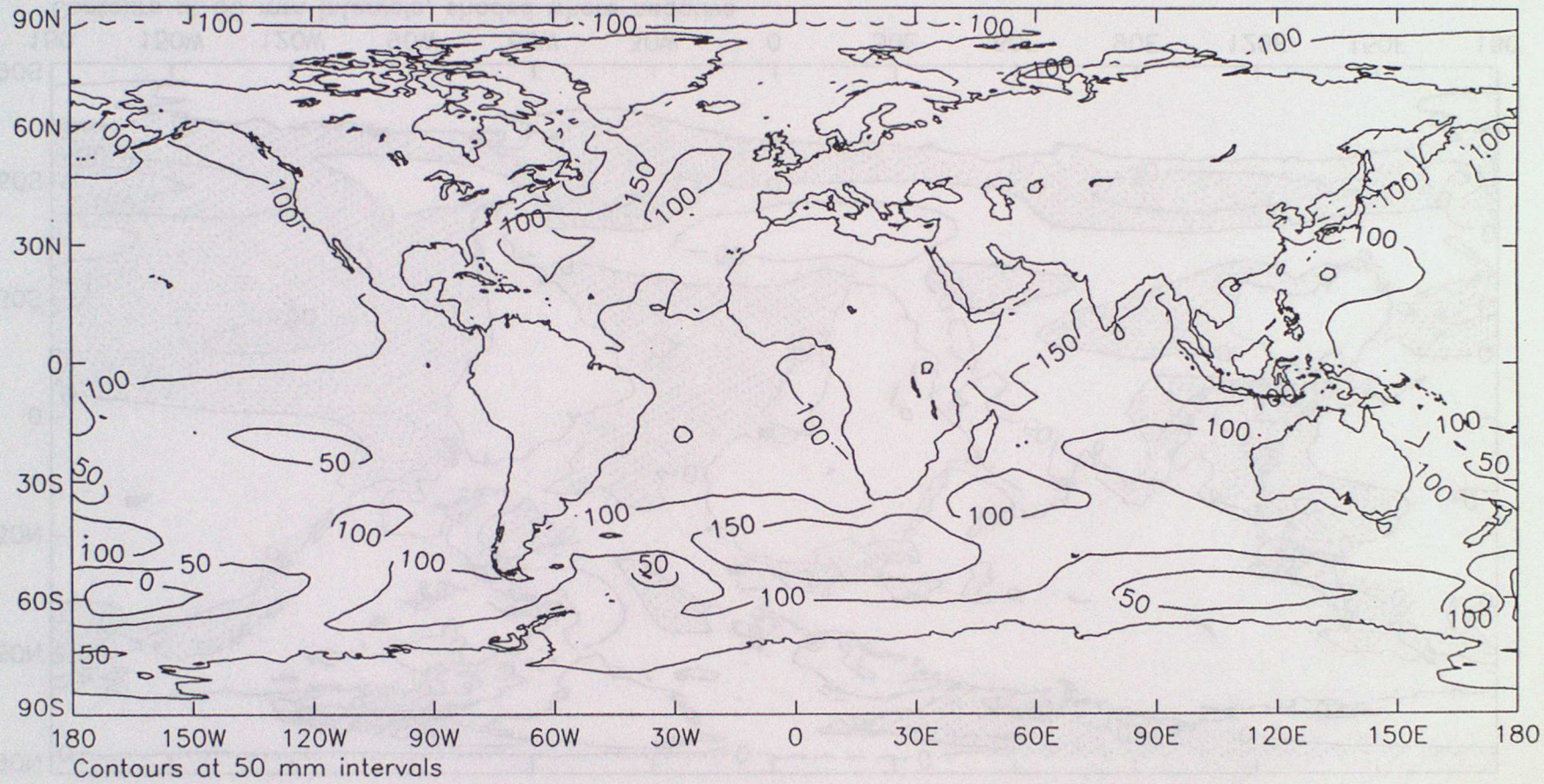
90N
60N
30N
0
30S
60S
90S
180
150W
120W
90W
60W
30W
0
30E
60E
90E
120E
150E
180
Contours at 50 mm intervals

Figure 9

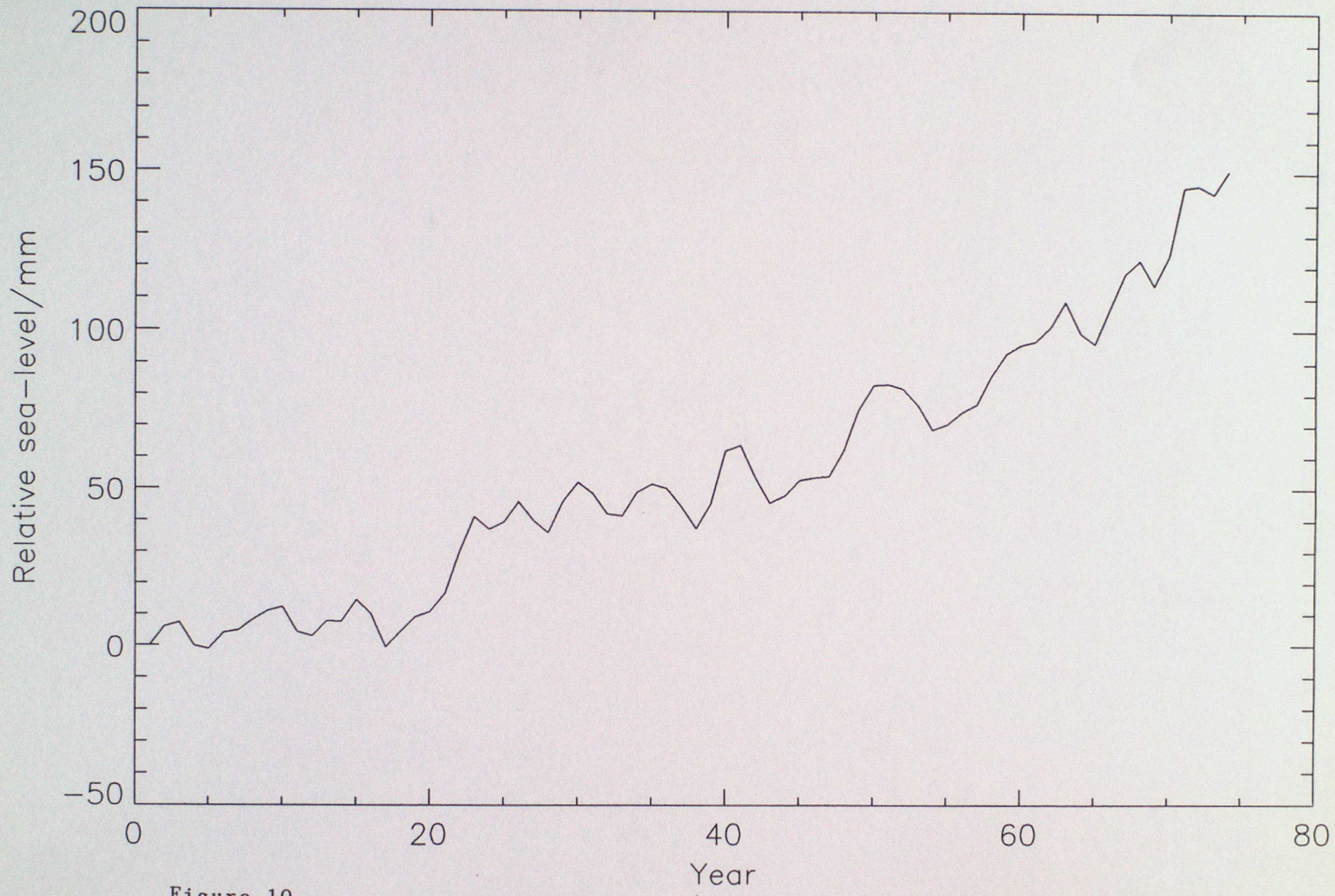

Figure 10

CLIMATE RESEARCH TECHNICAL NOTES

CRTN 1	Oct 1990	Estimates of the sensitivity of climate to vegetation changes using the Penman-Monteith equation. P R Rowntree
CRTN 2	Oct 1990	An ocean general circulation model of the Indian Ocean for hindcasting studies. D J Carrington
CRTN 3	Oct 1990	Simulation of the tropical diurnal cycle in a climate model. D P Rowell
CRTN 4	Oct 1990	Low frequency variability of the oceans. C K Folland, A Colman, D E Parker and A Bevan
CRTN 5	Dec 1990	A comparison of 11-level General Circulation Model Simulations with observations in the East Sahel. K Maskell
CRTN 6	Dec 1990	Climate Change Prediction. J F B Mitchell and Qing-cun Zeng
CRTN 7	Jan 1991	Deforestation of Amazonia - modelling the effects of albedo change. M F Mylne and P R Rowntree
CRTN 8	Jan 1991	The role of observations in climate prediction and research. D J Carson
CRTN 9	Mar 1991	The greenhouse effect and its likely consequences for climate change. D J Carson
CRTN 10	Apr 1991	Use of wind stresses from operational N.W.P. models to force an O.G.C.M. of the Indian Ocean. D J Carrington
CRTN 11	Jun 1991	A new daily Central England Temperature series, 1772-1991. D E Parker, T P Legg and C K Folland
CRTN 12	Jul 1991	Causes and predictability of Sahel rainfall variability. D P Rowell, C K Folland, K Maskell, J A Owen, M N Ward

CLIMATE RESEARCH TECHNICAL NOTES

CRTN 13	Jul 1991	Modelling changes in climate due to enhanced CO2, the role of atmospheric dynamics, cloud and moisture. C A Senior, J F B Mitchell, H Le Treut and Z-X Li
CRTN 14	Sep 1991	Sea temperature bucket models used to correct historical SST data in the Meteorological Office. C K Folland
CRTN 15	Aug 1991	Modelling climate change, and some potential effects on agriculture in the U.K. P R Rowntree, B A Callander and J Cochrane
CRTN 16	Aug 1991	The Boreal Forests and Climate G Thomas and P R Rowntree
CRTN 17	Aug 1991	Development of a Stratosphere-Troposphere Data Assimilation System. R Swinbank.
CRTN 18	Sep 1991	A study of asynchronous coupling using a simple climate model. M K Davey.
CRTN 19	Sep 1991	The Oceanic Carbon Cycle. N K Taylor
CRTN 20	Nov 1991	Worldwide ocean-atmosphere surface fields in Sahel wet and dry years using provisionally corrected surface wind data. M N Ward
CRTN 21	Dec 1991	Coupled tropical ocean global atmosphere models at the UKMO. M K Davey, C Gordon, S Ineson and S Lawrence
CRTN 22	Dec 1991	Empirical parameterisation of tropical ocean-atmosphere coupling. M Allen, M K Davey, D L T Anderson and P D Killworth
CRTN 23	Feb 1992	The temporal evolution of Equatorial Currents in the Indian Ocean D L T Anderson, D J Carrington, R A Corry and C Gordon
CRTN 24	Feb 1992	Stratospheric analyses provided by the U.K. Meteorological Office M J Bailey, A O'Neill and V D Pope

CLIMATE RESEARCH TECHNICAL NOTES

CRTN 25	Feb 1992	Modelling interannual variability in the Indian Ocean using momentum fluxes from the UKMO and ECMWF operational weather analyses. D L T Anderson and D J Carrington
CRTN 26	Mar 1992	A GCM simulation of the impact of Amazonian deforestation on climate using an improved canopy representation J Lean and P R Rowntree
CRTN 27	Mar 1992	The parameterization of rainfall interception in GCMs A J Dolman and D Gregory
CRTN 28	Jun 1992	Development of worldwide marine data eigenvectors since 1985 A W Colman
CRTN 29	Jun 1992	A tropical ocean model with reduced physics M K Davey
CRTN 30	Jun 1992	International Temperature Workshop, Boulder, Colorado, USA, 16 January 1992 Edited by D E Parker
CRTN 31	Jul 1992	Simulation of clear-sky outgoing longwave radiation over the oceans using operational analyses A Slingo and M J Webb
CRTN 32	Sep 1992	A prediction of the transient response of climate J M Murphy
CRTN 33	Nov 1992	LEPS scores for assessing climate model simulations and long-range forecasts. C K Folland
CRTN 34	Jan 1993	Stratospheric Data Assimilation System Guide Editer: R Swinbank
CRTN 35	Mar 1993	A Stratosphere-Troposphere Data Assimilation System R Swinbank and A O'Neill
CRTN 36	Mar 1993	Validation of hydrological schemes for climate models against catchment data. P R Rowntree and J Lean

CLIMATE RESEARCH TECHNICAL NOTES

CRTN 37	Apr 1993	Modelling of palaeoclimates: Examples from the recent past J F B Mitchell
CRTN 38	May 1993	A simulation of seasonality in ENSO forecast skill M K Davey, D L T Anderson and S Lawrence
CRTN 39	Jul 1993	ENSO Prediction experiments using a simple ocean-atmosphere model D-H Wu, D L T Anderson and M K Davey
CRTN 40	Sep 1993	Diagnosis of dynamic sea-surface and sea-level changes from the Cox ocean model J M Gregory
CRTN 41	Sep 1993	Seasonal variations of the clear-sky greenhouse effect: the role of changes in atmospheric temperatures and humidities M J Webb, A Slingo and G L Stephens
CRTN 42	Nov 1993	Sea-level changes under increasing atmospheric CO_2 in a transient coupled ocean-atmosphere GCM experiment. J M Gregory